MSC-05543

NASA CR-
141912

SKYLAB PROGRAM

EARTH RESOURCES EXPERIMENT PACKAGE

GROUND TRUTH DATA
FOR TEST SITES (SL-4)

CONTRACT NAS8-24000
AMENDMENT JSC-14S

National Aeronautics and Space Administration

LYNDON B. JOHNSON SPACE CENTER

Houston, Texas

APRIL 30, 1974

MSC-05543

GROUND TRUTH DATA

FOR TEST SITES (SL-4)

Approved by:

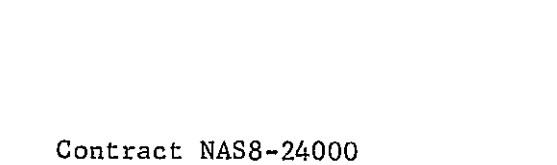

Richard A. Moke
Manager, System Analysis and
Integration Office, JSC/HC

Contract NAS8-24000
Amendment JSC-14S

Skylab Program
Lyndon B. Johnson Space Center

FOREWORD

This document is submitted by Martin Marietta Corporation in accordance with the requirements of Annex I to Exhibit A, Statement of Work, Part I, Data Requirements List (DRL), of Contract NAS8-24000, Amendment JSC-14S, Line Item 296, and was performed under WBS-02216.

The work was performed by R. L. Hustrom and any inquiries should be addressed to him at (303) 794-5211, Ext. 3808. After June 30, 1974, inquiries should be addressed to NASA JSC, Earth Resources Program Office, Mail Code HA.

CONTENTS

1. INTRODUCTION

During the SL-4 Skylab mission, field measurements were performed simultaneous with Skylab overpasses in order to provide comparative calibration and performance evaluation measurements for the EREP sensors: Wavelength regions covered were solar - 400 to 1300 nanometer (nm) - and the thermal - 8 to 14 micrometer (μm) - radiation regions. Similar measurements were also performed on the SL-2 and SL-3 mission.- "Ground Truth Data for Test Sites (SL-2 and SL-3)", Report Nos. MSC-05531 and MSC-05537, NAS8-24000, Amendment JSC-14S.

Sites employed for the thermal radiation brightness temperature measurements consisted of, (1) snow sites - Rio Grande and Dillon Reservoirs, Colorado (2) warm water lakes - Laguna Reservoir, Arizona, and the Great Salt Lake, Utah; (3) cold water lakes - Walker Lake and Lake Mead, Nevada; (4) a dry lake bed - Katherine Playa, New Mexico; and (5) a geothermal site* - The Geysers, California.

Sites employed for the solar radiation region, consisted of the Great Salt Lake Desert, Utah, and Katherine Playa, New Mexico.

Measurements consisted of general conditions and near surface meteorology (wind,temperature, pressure, etc.) for all sites. Measurements at the thermal sites consisted of atmospheric temperature and humidity vs altitude, taken with a radiosonde, and the thermal brightness temperature (8-14 μm). Measurements at the solar radiation sites consisted of total and diffuse solar radiation, direct solar radiation(subsequently analyzed for optical depth/transmittance),and target reflectivity/radiance. The particular instruments used are discussed in the following sections, along with analyses performed. Detailed instrument

* Included in this report for general information only, Geysers effort was authorized by NASA JSC under a separate work statement (report MSC-05538).

operation, calibrations, techniques, and errors, are given in the Appendix.

The purpose of this report is to present the measurements and analyses made, how they were made, calibrations and analyses performed, techniques used, and results obtained. It is not within the scope of the work performed to interpret the measurements, calculations, results, etc., in terms of the detailed physical nature of the targets, the atmosphere, etc.

2. THERMAL INFRARED CALIBRATION MEASUREMENTS AND ANALYSES

2.1 Instrumentation and Techniques - The thermal brightness temperature, from 8 to 14 μm broadband, of the targets were measured with a Barnes Precision Thermal Radiometer, Model PRT-5. Where possible, the PRT-5 was flown on a helicopter in order to determine the spatial nature of the targets temperature; plus, derive an integrated temperature over a large resolution element. The PRT-5 has a sensitivity range of $-20^{o}C$ to $+ 75^{o}C$, a FOV of 2^{o}, an accuracy of $.5^{o}C$, and a stability of .1%. The instrument used was calibrated by the Martin Marietta Calibration Laboratory, details are given in the Appendix.

The temperature and humidity profiles were measured with a Colspan (Boulder, CO.) radiosonde (rocket and balloon) system. This system uses a small electronics package, containing a bead thermistor and standard (ML-475) carbon element hygristor, that telemeters (as it descends on a parachute) data to a ground receiver (403 MHz). A net temperature error of $\pm$ $.3^{o}C$ exists, and a net humidity error of $\pm$ 5.5% R.H. exists. A slight error in altitude position exists because of the combination of the sensors response time and the descent rate (25 ft/sec) of the parachute. For the temperature profile the error is $\pm$ 32 ft., and for the humidity sensor a $\pm$ 19 ft. error exists. The calibration

and analysis technique used are given in the Appendix.

The near surface meteorology measurements were made with a sling psychrometer (wet and dry bulb temperature, $1^{o}F$ accuracy), a cup anemometer ($\pm$ 2 m.p.h. accuracy), and a aneroid barometer ($\pm$ .1 inch accuracy).

2.2 Measurements and Analyses

2.2.1 THE GEYSERS, CALIFORNIA, 18 DEC. 1973

Site Coordinates: $38^{o}45'38"$ N Latitude
$122^{o}47'37"$ W Longitude

SREP Pass: Track 63, Pass No. 68, Rev. 3145

Time of Overpass: 352:11:36:11 GMT
0436 PDT, Local

2.2.1.1 General Conditions - Pre-dawn, generally clear in Geysers area, ground fog in lower Big Sulfur Creek valley.

2.2.1.2 Near Surface Meteorology - Dry bulb temperature = $8.33^{o}C$; wet bulb temperature = $6.11^{o}C$; surface pressure = 712.5 mm of Hg (from U.S. Standard Atmosphere); wind-calm.

2.2.1.3 Temperature and Humidity Profile*

2.2.1.4 Brightness Temperature*

2.2.2 RIO GRANDE RESERVOIR, COLORADO, 14 JAN. 1974

Site Coordinates: $37^{o}43'45"$ N Latitude
$107^{o}17'30"$ W Longitude

* The detailed analyses of this data is covered by a separate statement of work and will be reported in a later document, Report No. MSC-05538.

EREP Pass: Track 30, Pass No. 83, Rev. 3538

Time of Overpass: 014:16:00:26 GMT
1000 MDT, Local

2.2.2.1 General Conditions - Extensive snow cover, low cirrus clouds near 20,000 ft. A.S.L. (60% scattered coverage) periodically shading area.

2.2.2.2 Near Surface Meteorology - Dry bulb temperature = -8.33°C; wet bulb temperature = not obtainable; surface pressure = 544.0 mm of Hg (measured); wind-calm.

2.2.2.3 Brightness Temperature - The brightness temperature was measured with a PRT-5 radiometer, flown in a helicopter. The results are shown in Figure 1.

2.2.3 LAGUNA RESERVOIR AND IMPERIAL DAM, ARIZONA, 26 JAN.1974

Site Coordinates: 32°50'00" N Latitude
114°20'00" W Longitude

EREP Pass: Track 63, Pass No. 91, Rev. 3713

Time of Overpass: 0 26:19:43:30 GMT
1243 MST, Local

2.2.3.1 General Conditions - Clear

2.2.3.2 Near Surface Meteorology - Dry bulb = 19.4°C; wet bulb = 12.8°C; surface pressure = 759 mm of Hg (measured); wind - 10 mph/SW.

2.2.3.3 Brightness Temperature - The brightness temperature of Laguna Reservoir and nearby Imperial Reservoir are shown in Figures 4 and 5.

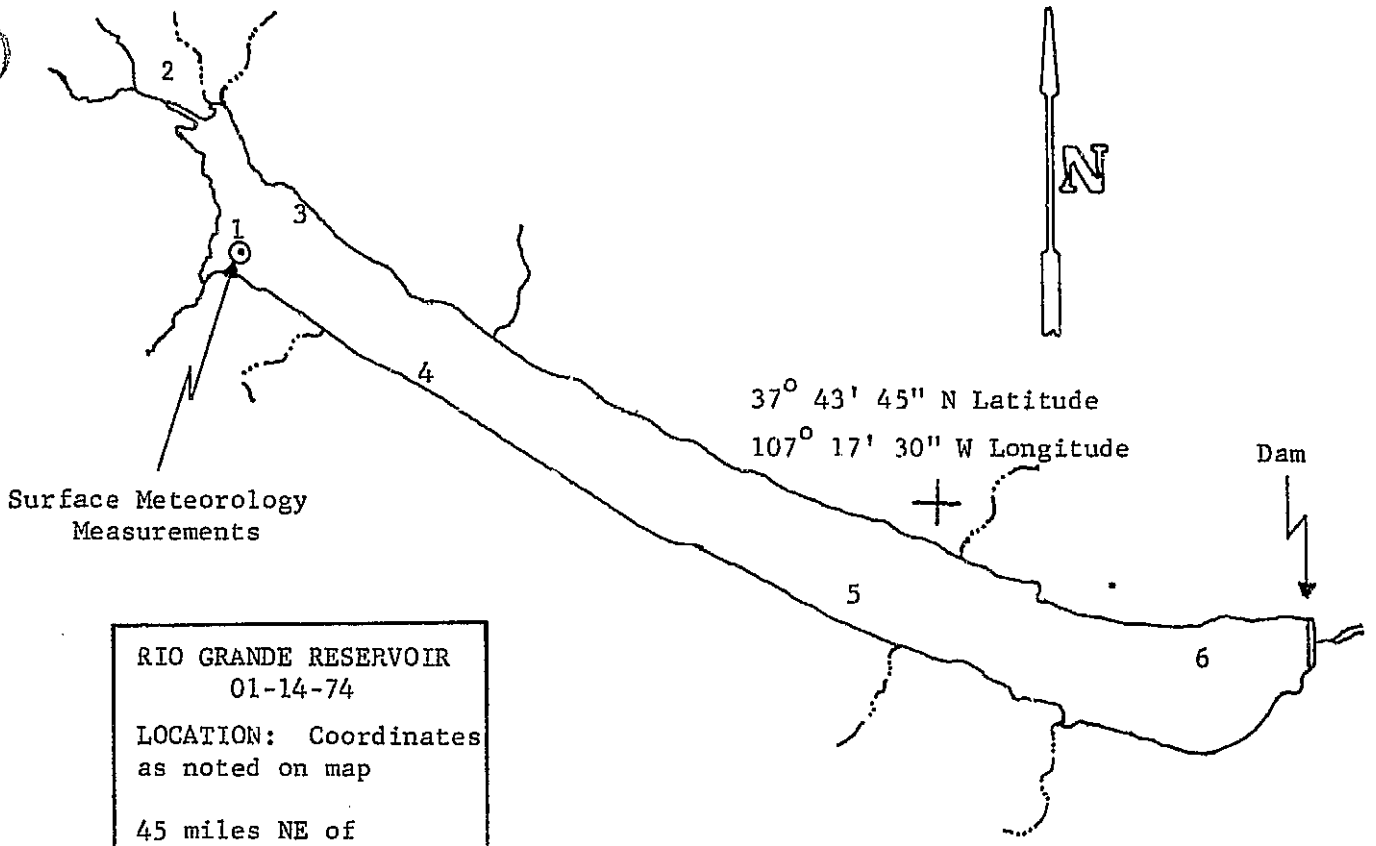

RIO GRANDE RESERVOIR
01-14-74

LOCATION: Coordinates as noted on map

45 miles NE of Durango, Colo.

SCALE: 1:48000

ELEVATION: 9400 ft. A.S.L.

SNOW BRIGHTNESS TEMPERATURE						
Position	Helicopter Elevation	Time (MDT)		°C	Comments	
1	On Surface	1045		-13.0		
2	9,500	1047		-18.5		
3	9,600	1048		-18.0		
3	9,900	1049		-16.5		
2	10,400	1051		-15.0		
3	10,400	1052		-14.0		
4	10,400	1053		-16.0		
5	10,400	1054		-16.5		
6	10,400	1055		-16.0		

Fig. 1: Rio Grande Reservoir, CO, Snow Brightness Temperature and Lake Location Map, 14 January 1974

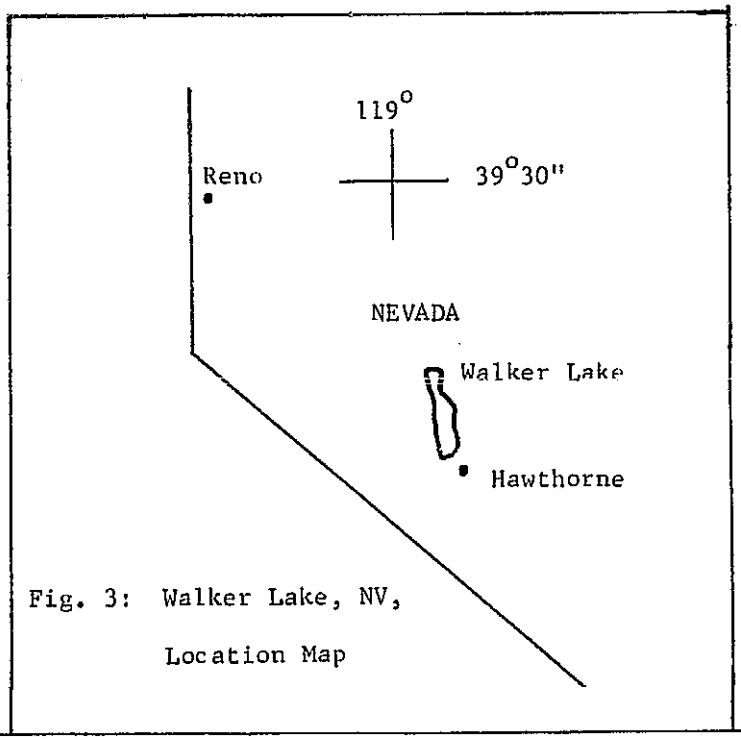

Fig. 3: Walker Lake, NV, Location Map

Fig. 2: Laguna Reservoir, AZ, Location Map

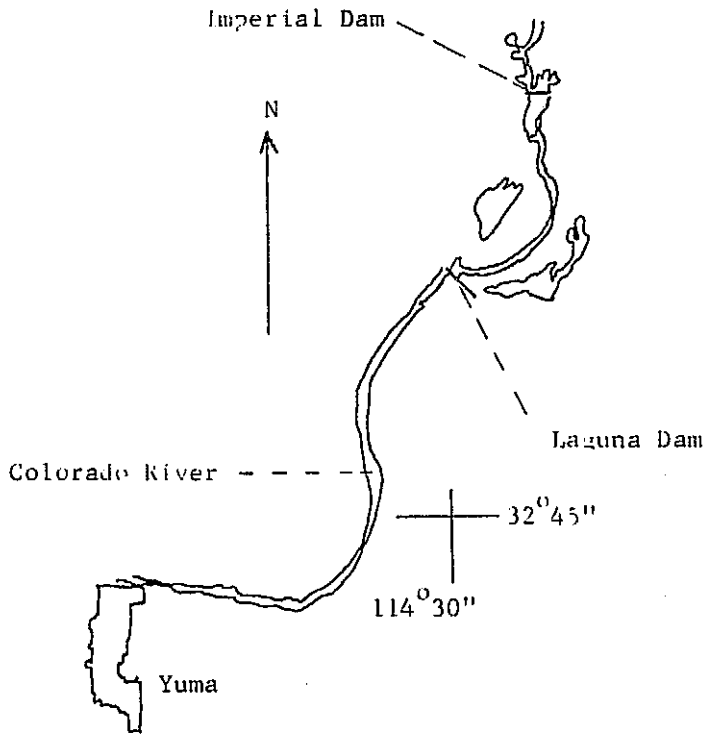

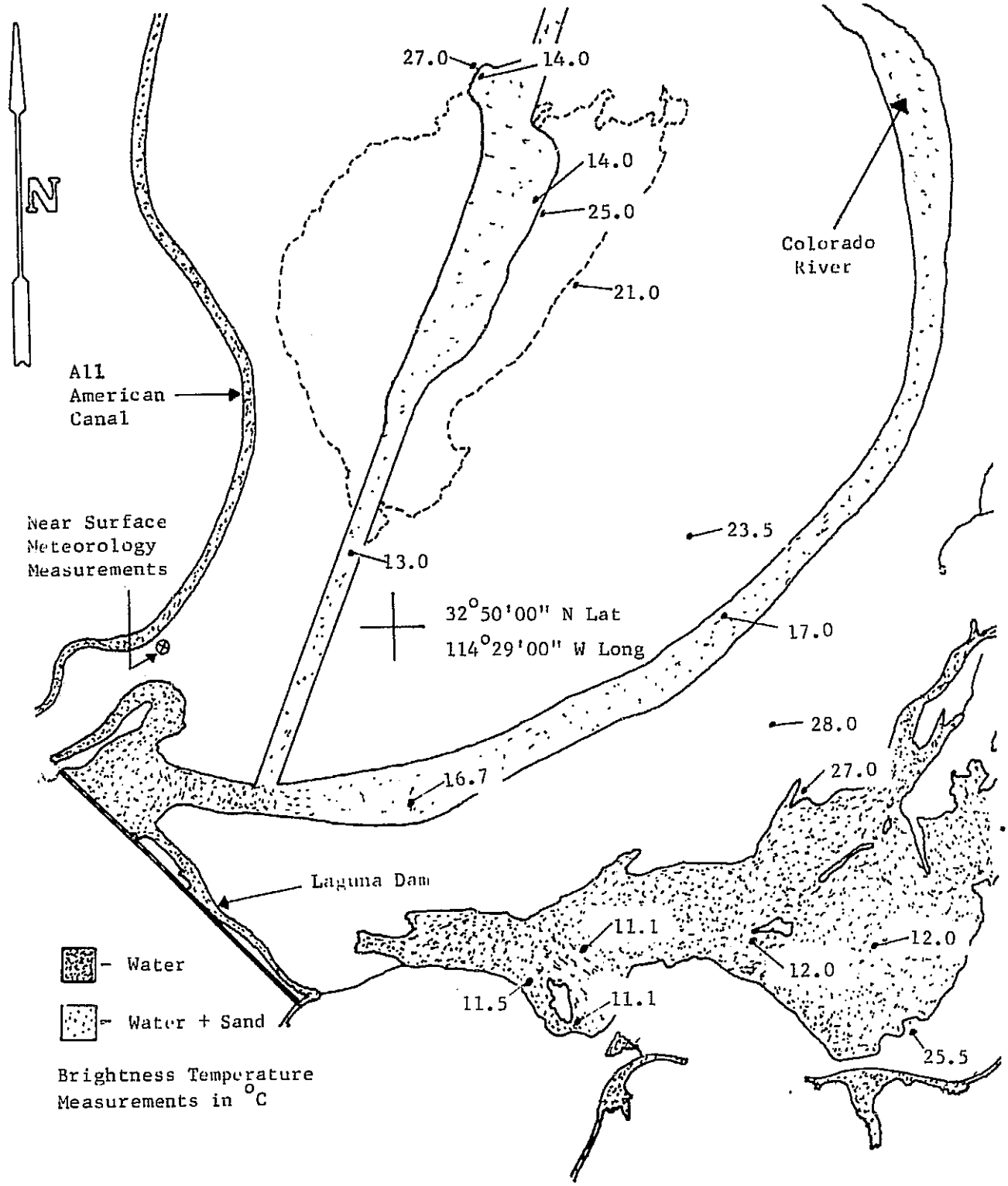

Fig. 4: Laguna Reservoir, AZ, Thermal Brightness Temperature Location, 26 January 1974

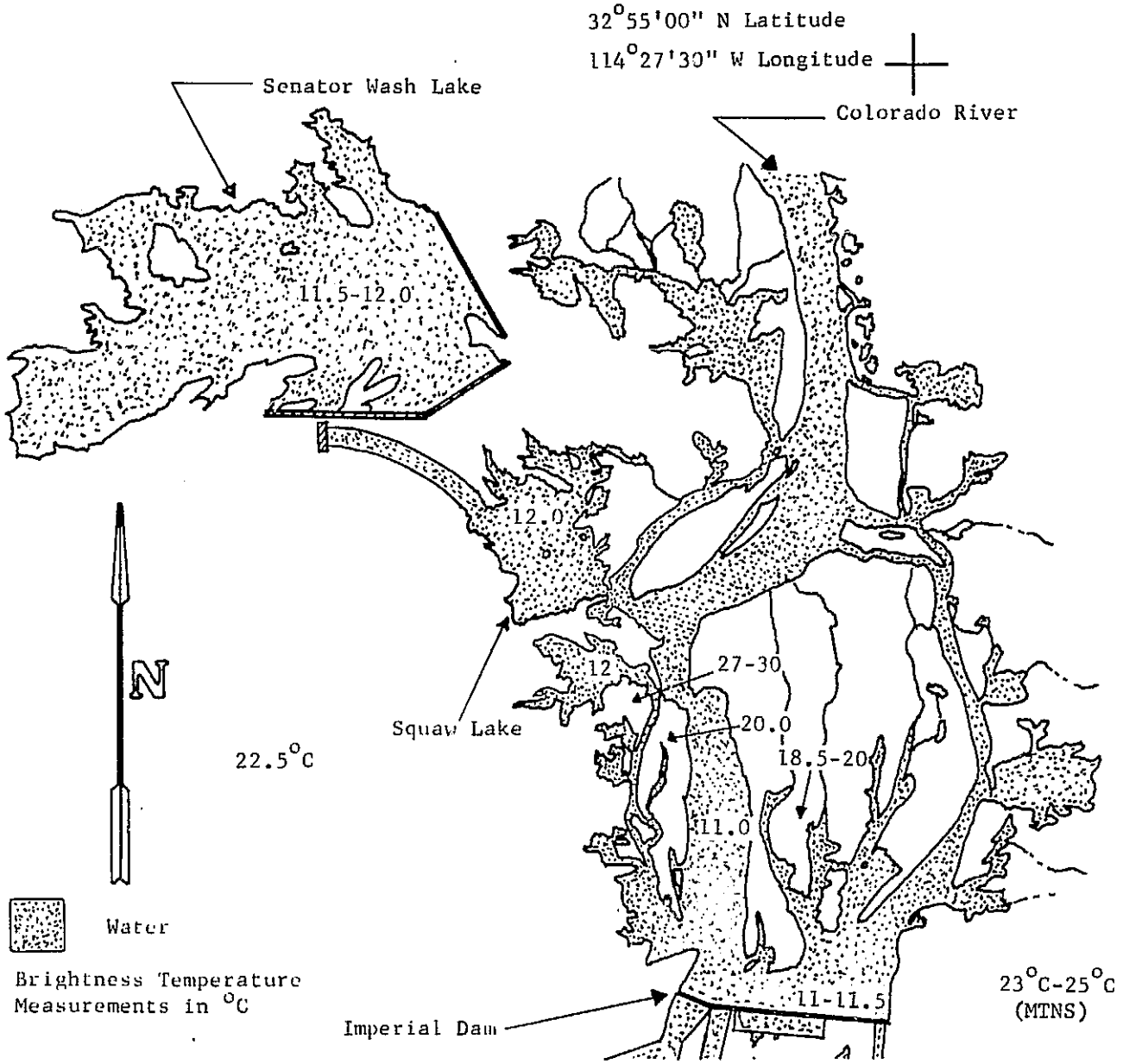

Fig. 5: Imperial Dam, AZ, Thermal Brightness Temperature Location, 26 January 1974

2.2.4 THE GEYSERS, CALIFORNIA, 26 JAN. 1974

Site Coordinates: 38°45'38" N Latitude
122°47'37" W Longitude

EREP Pass: Track 63, Pass No. 91, Rev. 3713

Time of Overpass: 026:19:41:20
1241 PDT, Local

2.2.4.1 General Conditions - Clear

2.2.4.2 Near Surface Meteorology - Dry bulb temperature - 10.0°C; wet bulb temperature = 5.6°C; surface pressure = 718 mm of Hg (measured); wind = 3.5 mph/N.

2.2.4.3 Temperature and Humidity Profile*

2.2.4.4 Brightness Temperature*

2.2.5 WALKER LAKE, NEVADA, 27 JAN. 1974

Site Coordinates: 38°45'00" N Latitude
118°45'00" W Longitude
(see Figure 3)

EREP Pass: Track 06, Pass No. 93
Rev. 3727

Time of Overpass: 027:17:58:42 GMT
1058 PDT, Local

2.2.5.1 General Conditions - 70% stratus cloud cover.

2.2.5.2 Near Surface Meteorology - Dry bulb temperature = 4.4°C; wet bulb temperature = 1.7°C; surface pressure - 663 mm of Hg (measured); wind = <2 mph/S.

2.2.5.3 Temperature and Humidity Profile - This data not reduced due to 70% cloud cover.

---

* The detailed analyses of this data is covered by a separate statement of work and will be reported in a later document, Report No. MSC-05538.

2.2.5.4 Brightness Temperature - The brightness temperature, as measured with a PRT-5 radiometer aboard a helicopter, is 6-7°C over water and 10-12°C over surrounding land.

2.2.6 GREAT SALT LAKE, UTAH, 29 JAN. 1974

Site Coordinates:	41°15'00" N Latitude 112°45'00" W Longitude
EREP Pass:	Track 34, Pass No. 95, 1132 MDT, Local
Time of Overpass:	029:17:32:47 GMT 1132 MDT, Local

2.2.6.1 General Conditions - Scattered Cirrus clouds.

2.2.6.2 Near Surface Meteorology - Dry bulb temperature = -1.39°C; wet bulb temperature =-2.22°C; surface pressure = 650 mm of Hg (measured); wind - calm.

2.2.6.3 Temperature and Humidity Profile - This data not reduced due to excessive cloud cover.

2.2.6.4 Brightness Temperature - The brightness temperature, as measured with a PRT-5 radiometer aboard a helicopter, is shown in Figure 6.

2.2.7 DILLON RESERVOIR, COLORADO, 30 JAN. 1974

Site Coordinates:	39°31'12" N Latitude 106°03'10" W Longitude
EREP Pass:	Track 48, Pass No. 96, Rev. 3769
Time of Overpass:	030:16:50:49 GMT 1050 MDT, Local

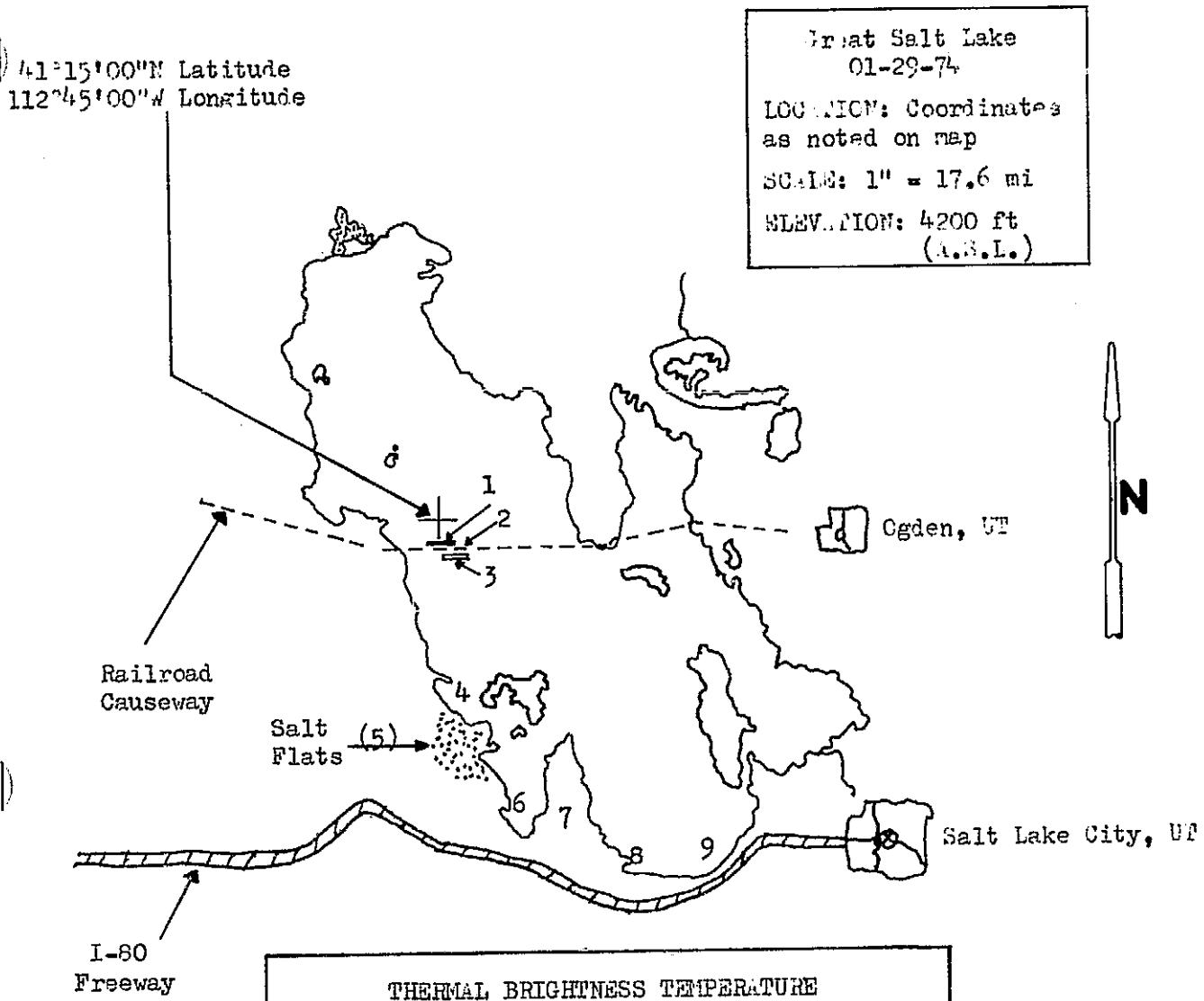

THERMAL BRIGHTNESS TEMPERATURE			
Position	Elevation (A.S.L.)	Temperature (°C)	Comments
1	5200 ft	4.5- 6	
2	5200	7 - 9	On Causeway
3	5200	5	
4	5200	5.5- 6	
5	5200	10	
6	5200	5 - 6	
7	5200	10 -11	
8	5200	4.5	
9	5200	5.5	

Fig. 6: Great Salt Lake, UT, Thermal Brightness Temperature and Lake Location Map, 29 January 1974

2.2.7.1 General Conditions - Scattered, high, cirrus clouds.

2.2.7.2 Near Surface Meteorology - Dry bulb temperature = -0.3°C; wet bulb temperature = not obtainable; surface pressure = 544 mm of Hg (from U.S. Standard Atmosphere); wind - 12 mph/N.

2.2.7.3 Temperature and Humidity Profile - The temperature profile is shown in Figure 8, and is listed in Table 1. The humidity profile is shown in Figure 9, and is listed in Table 2.

2.2.7.4 Brightness Temperature - The brightness temperature of the snow was measured at ground level in the area shown in Figure 7, and found to be -6.2 ± .2°C

2.2.8 LAKE MEAD, NEVADA, 01 FEB 1974

Site Coordinates:	36°07'30" N Latitude 114°37'30" W Longitude
EREP Pass:	Track 06, Pass No. 98, Rev. 3798
Time of Overpass:	032:1700:36 GMT 1000 PDT, Local

2.2.8.1 General Conditions - Clear

2.2.8.2 Near Surface Meteorology - Dry bulb temperature = 11.1°C; wet bulb temperature = not obtained ; surface pressure = 724.0 mm of Hg (measured);wind - calm.

2.2.8.3 Brightness Temperature - The brightness temperature was measured with a PRT-5 radiometer, aboard a small aircraft; the results are shown in Figure 10.

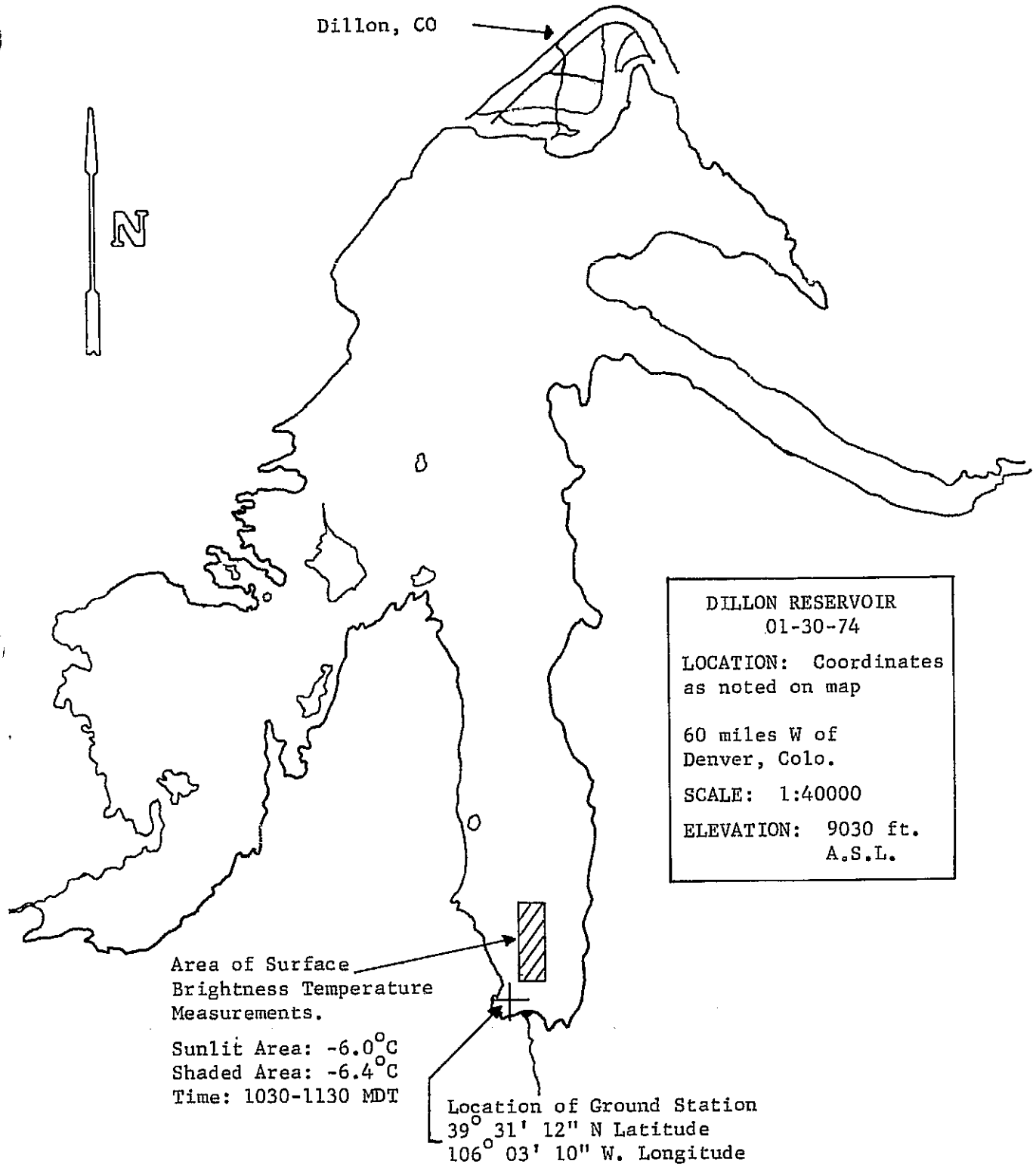

Fig. 7: Dillon Reservoir, CO, Snow Brightness Temperature and Lake Location Map, 30 January 1974

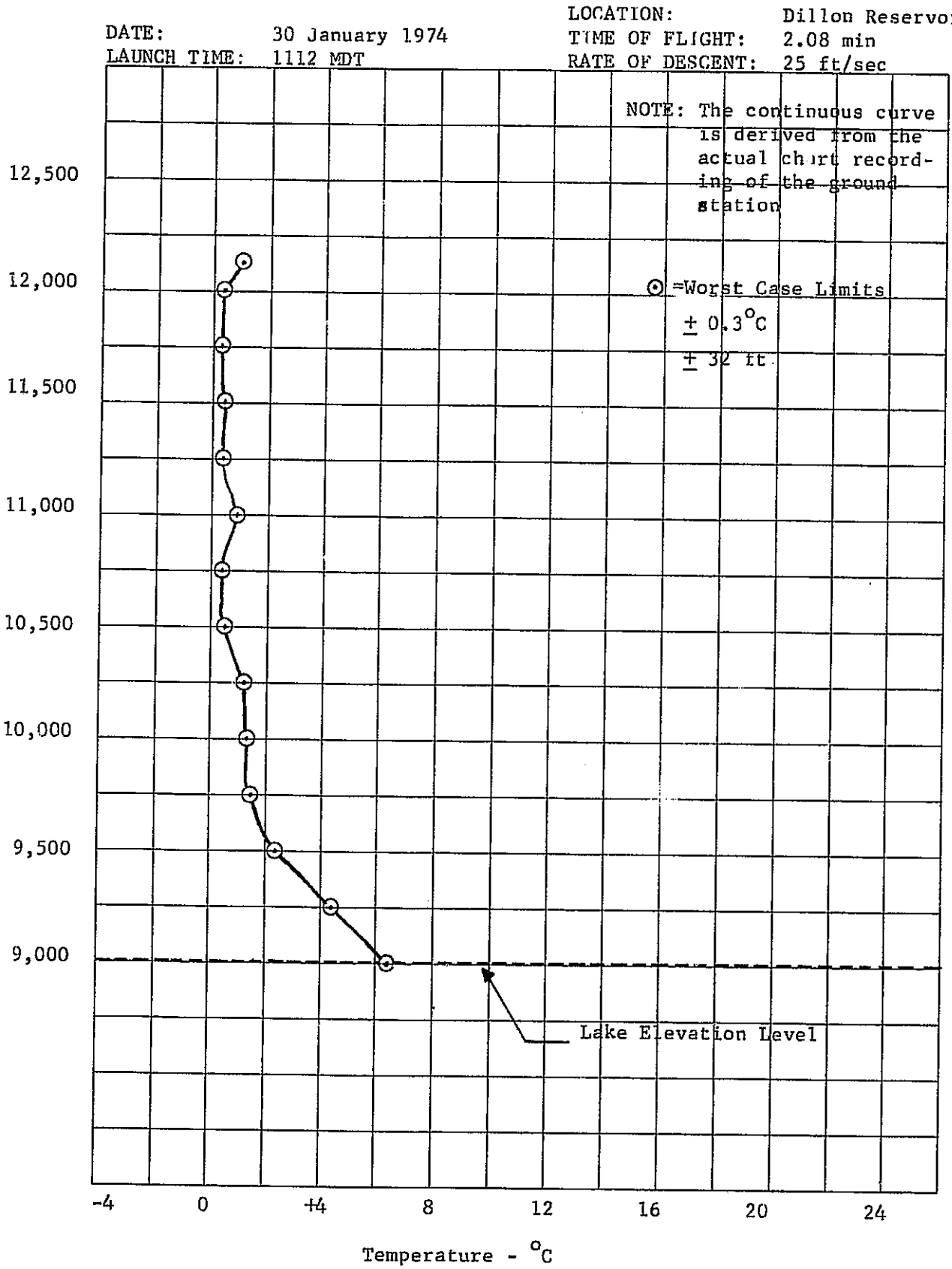

Fig. 8: Dillon Reservoir, CO, Radiosonde Temperature Profile Plot for 30 January 1974

RADIOSONDE EVALUATION DATA

# of ¼" from Drop	Raw Data from St.CH.	Time from Drop	Altitude Ref:12125'	Altitude (A.S.L.)	Temperature from Chart	Comments
0	4- 38.5	0 sec.	0 ft.	12125 ft.	1.0 °C	Stabilize
2	4- 35.0	2.5	- 125	12000	0.4	
6	4- 34.5	15.0	- 375	11750	0.3	
10	4- 35.0	25	- 625	11500	0.4	
14	4- 35.0	35	- 875	11250	0.4	
18	4- 38.0	45	-1125	11000	0.9	
22	4- 35.0	55	-1375	10750	0.4	
26	4- 35.5	65	-1625	10500	0.5	
30	4- 40.0	75	-1875	10250	1.2	
34	4- 40.5	85	-2125	10000	1.3	
38	4- 41.5	95	-2375	9750	1.5	
42	4- 46.5	105	-2625	9500	2.3	
46	5- 9.7	115	-2875	9250	4.4	
50	5- 21.5	125	-3125	9000	6.4	Ground Contact

DATE 01-30-74 LOCATION Dillon Reservoir, CO

NOTES: 1) Recorder travels at 2.5 sec/¼" Div
2) Radiosonde launched at 1112 MDT, approximately 20 seconds later sonde separated from rocket and sensors stabilized 10 seconds following separation.
3) Descent rate was 25 ft/sec.

Table 1: Dillon Reservoir, CO, Radiosonde Temperature Profile Listing for 30 January 1974

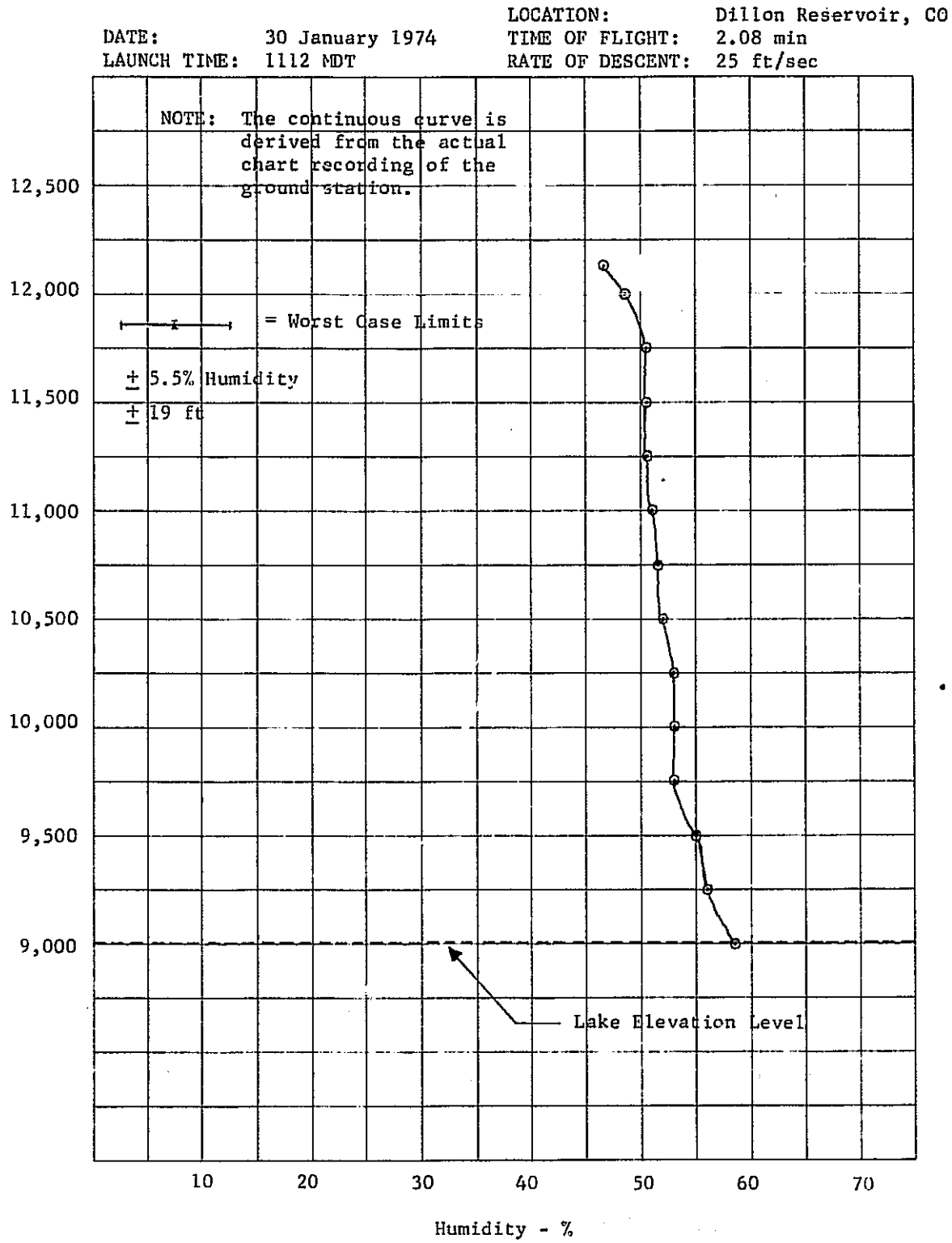

Fig. 9: Dillon Reservoir, CO, Radiosonde Humidity Profile Plot for 30 January 1974

RADIOSONDE EVALUATION DATA

# of ½" from Drop	Raw Data from ST.CH.	Time from Drop	Altitude Ref:12125'	Altitude (A.S.L.)	Humidity from Chart	Comments
0	1- 40.0	0 sec.	0 ft.	12125 ft.	46.5%	Stabilize
2	1- 44.5	2.5	- 125	12000	48.5	
6	1- 49.0	15.0	- 375	11750	50.5	
10	1- 49.0	25	- 625	11500	50.5	
14	1- 49.0	35	- 875	11250	50.5	
18	2- 1.0	45	-1125	11000	51.0	Scale Change
22	2- 3.5	55	-1375	10750	51.5	
26	2- 5.0	65	-1625	10500	52.0	
30	2- 6.5	75	-1875	10250	53.0	
34	2- 8.0	85	-2125	10000	53.0	
38	2- 7.0	95	-2375	9750	53.0	
42	2- 15.0	105	-2625	9500	55.0	
46	2- 17.0	115	-2875	9250	56.0	
50	2- 25.0	125	-3125	9000	58.5	Ground Contact

DATE 01-30-74 LOCATION Dillon Reservoir, CO

NOTES: 1) Recorder travels at 2.5 sec/½" Div.
2) Radiosonde launched at 1112 MDT, approximately 20 seconds later sonde separated from rocket and sensors stabilized 10 seconds following separation.
3) Descent rate was 25 ft/sec.

Table 2: Dillon Reservoir, CO, Radiosonde Humidity Profile Listing for 30 January 1974

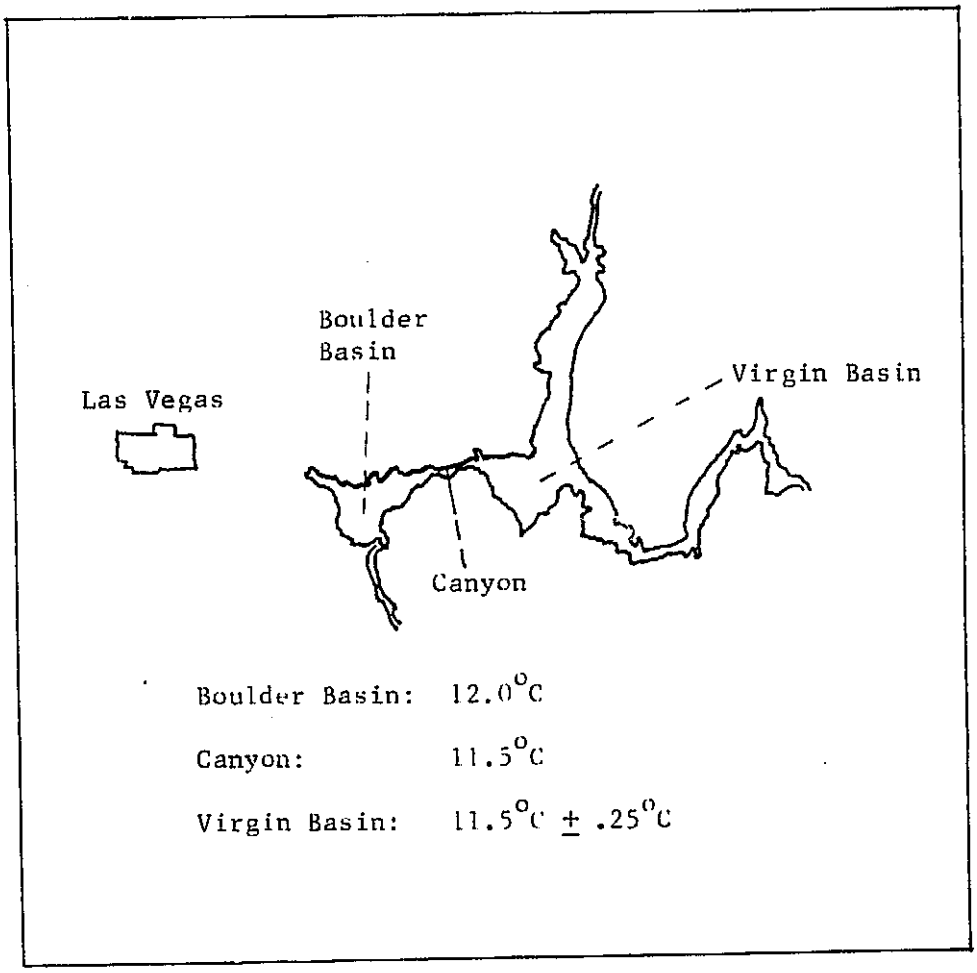

Fig. 10: Lake Mead, NV, Thermal Brightness Temperature and Lake Location Map, 01 February 1974

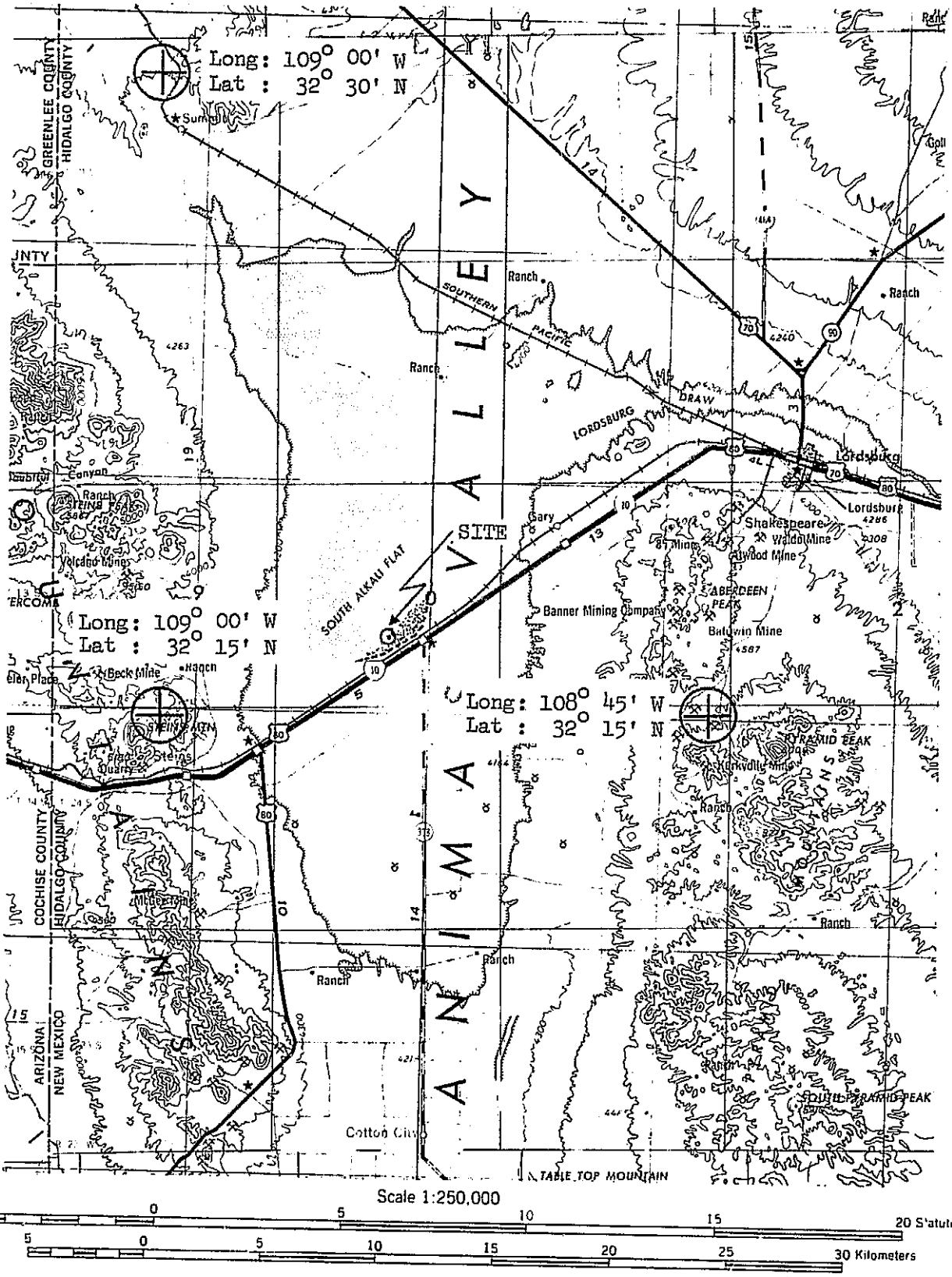

Fig. 11: Katherine Playa, NM, Location Map

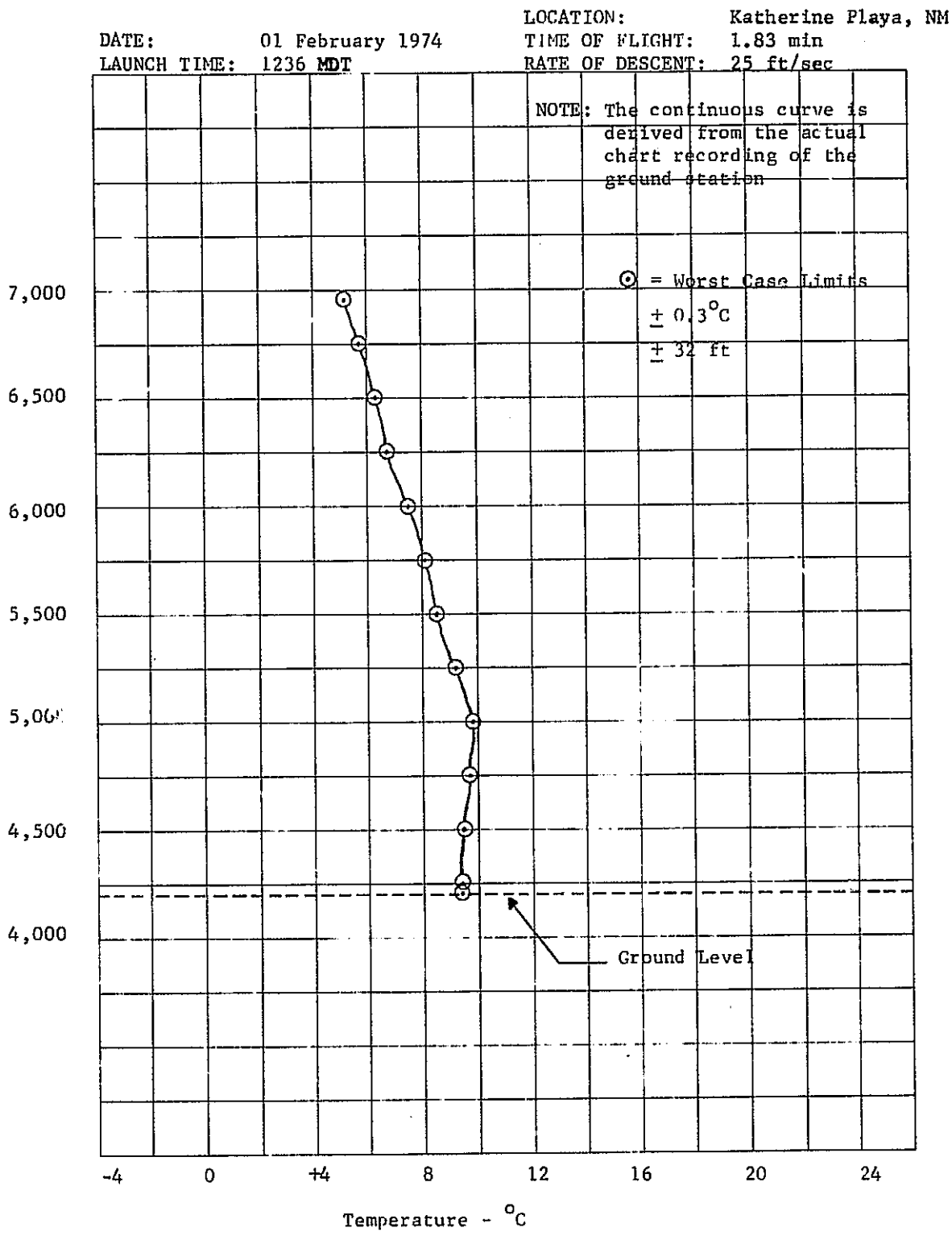

Fig. 12: Katherine Playa, NM, Radiosonde Temperature Profile Plot for 01 February 1974

RADIOSONDE EVALUATION DATA

# of ½" from Drop	Raw Data from ST. CH.	Time from Drop	Altitude Ref: 6950'	Altitude (A.S.L.)	Temperature from Table	Comments
0	5- 14.0	0 sec	000 ft	6950 ft	+ 5.2 °C	Drop
3.2	5- 17.5	8	- 200	6750	5.7	
7.2	5- 21.0	18	- 450	6500	6.3	
11.2	5- 23.5	28	- 700	6250	6.7	
15.2	5- 28.0	38	- 950	6000	7.5	
19.2	5- 31.5	48	- 1200	5750	8.1	
23.2	5- 34.2	58	- 1450	5500	8.5	
27.2	5- 38.0	68	- 1700	5250	9.2	
31.2	5- 41.5	78	- 1950	5000	9.8	
35.2	5- 41.0	88	- 2200	4750	9.7	
39.2	5- 39.8	98	- 2450	4500	9.5	
43.2	5- 39.5	108	- 2700	4250	9.4	
44.0	5- 39.2	110	- 2750	4200	9.4	Ground Contact

DATE 02-01-74 LOCATION Katherine Playa, NM

NOTES: 1) Recorder travels at 2.5 sec/½" div.
2) Normal drop; radiosonde descended at approximately 25 ft/sec.

Table 3: Katherine Playa, NM, Radiosonde Temperature Profile Listing for 01 February 1974

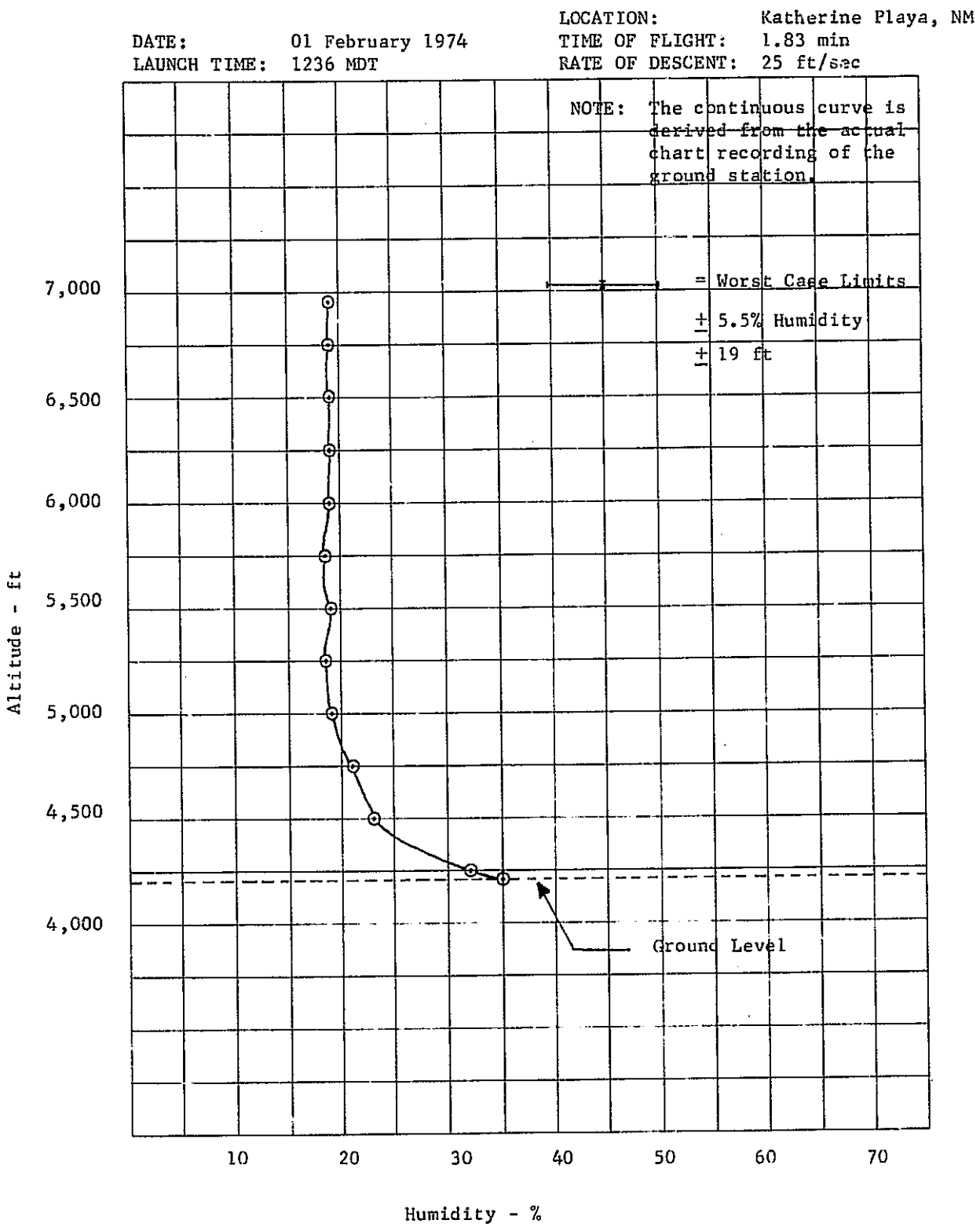

Fig. 13: Katherine Playa, NM, Radiosonde Humidity Profile Plot for 01 February 1974

RADIOSONDE EVALUATION DATA

# of ½" from Drop	Raw Data from ST.CH.	Time from Drop	Altitude Ref: 6950'	Altitude (A.S.L.)	Humidity from Table	Comments
0	2- 8.0	0 sec	000 ft	6950 ft	19%	Drop
3.2	2- 8.5	8	- 200	6750	19	[Humidities
7.2	2- 9.0	18	- 450	6500	19	derived
11.2	2- 8.0	28	- 700	6250	19	from table
15.2	2- 8.0	38	- 950	6000	19	below]
19.2	2- 7.5	48	- 1200	5750	18.5	
23.2	2- 8.0	58	- 1450	5500	19	
27.2	2- 7.5	68	- 1700	5250	18.5	
31.2	2- 8.5	78	- 1950	5000	19	
35.2	2- 11.0	88	- 2200	4750	21	
39.2	2- 12.5	98	- 2450	4500	23	
43.2	2- 20.0	108	- 2700	4250	32	
44.0	2- 25.0	110	- 2750	4200	35	Ground Contact

* Raw Data	X	Y	I	D.P.	Hum %	
2- 8.0	258.0	210.56	1	10.6	19	C_c/X_c =
2- 8.5	258.5	210.96	1	11.0	19	
2- 9.0	259.0	211.37	1	11.4	19	221.9/271.9 =
2- 8.0	258.0	210.56	1	10.6	19	0.8161
2- 8.0	258.0	210.56	1	10.6	19	
2- 7.5	257.5	210.148	1	10.1	18.5	
2- 8.0	258.0	210.56	1	10.6	19	
2- 7.5	257.5	210.148	1	10.1	18.5	
2- 8.5	258.5	210.96	1	11.0	19	
2- 11.0	261.0	213.00	1	13.0	21	
2- 12.5	262.5	214.23	1	14.3	23	
2- 20.0	270.0	220.35	1	20.4	32	
2- 25.0	275.0	224.43	1	24.3	35	

DATE 02-01-74 LOCATION Katherine Playa, NM

NOTES: 1) Recorder travels at 2.5 sec/½" div.
2) Normal drop; radiosonde descended at approximately 25 ft/sec.
*3) Field calibration was incorrect, therefore a correction factor must be applied and this was supplied by the vendor of the radiosonde. $X = [200 + 50(R-1)] + D.P. \Rightarrow Y = (C_c/X_c)X \Rightarrow Data' = (Y-350)/50 \Rightarrow I + Re$; where; R = Range; D.P. = Data Point; C_c = Correct Calib. (R = 1, D.P. = 21.9 ⇒ 221.9); X_c = X at incorrect calib. D.P.; Data' = Corrected Data Point; I = Integer ⇒ Corrected R; Re = Fractional Remainder ⇒ % of 50 D.P.'s of full scale.

Table 4: Katherine Playa, NM, Radiosonde Humidity Profile Listing for 01 February 1974

2.2.9 KATHERINE PLAYA, NEW MEXICO, 01 FEB 1974

Site Coordinates:	32°18'00" N Latitude 108°53'00" W Longitude
EREP Pass:	Track 06, Pass No. 98, Rev. 3798
Time of Overpass:	032:17:02:08 GMT 1102 MDT, Local

2.2.9.1 General Conditions - Clear

2.2.9.2 Near Surface Meteorology - Dry bulb temperature = 7.22°C; wet bulb temperature = 1.7°C; surface pressure = 662 mm of Hg (from U.S. Standard Atmosphere); wind - calm.

2.2.9.3 Temperature and Humidity Profile - The temperature profile is shown in Figure 12 , and is listed in Table 3 . The humidity profile is shown in Figure 13, and is listed in Table 4 .

2.2.9.4 Brightness Temperature - The brightness temperature was measured with a PRT-5 radiometer, at ground level. The brightness temperature of the playa surface was found to be $10 \pm 1^{\circ}C$.

3. SOLAR RADIATION CALIBRATION MEASUREMENTS AND ANALYSES

3.1 Instrumentation and Techniques - Two types of instrumentation were used to measure direct, diffuse, total and reflected solar radiation.

The first type of instruments used were two interference wedge, spectral scanning, spectroradiometers, manufactured by I.S.C.O (Instrumentation Specialties Company, Lincoln, Neb.). The wavelength covered was 400 to 1300 nm, with halfband widths of 15 nm, from 400 to 750 nm, and 30 nm from 750 to 1300 nm. The sensing element is a planor diode, with a teflon diffuser at the acceptance end of a fiber optics probe. One

I.S.C.O was used to periodically monitor ($\approx$1/2 hr. increments) the direct solar beam, with a 6^{o} collimator. The measurements were subsequently used to derive atmospheric optical depth, by using the Lambert/Beers Law method. The other I.S.C.O was used to measure the total (180^{o}) incident solar radiation and the diffuse (sky) radiation (180^{o}). The total was measured by positioning the teflon diffuser so that it viewed the entire upper hemisphere, making certain that the surface of the diffuser was horizontal. The diffuse (sky) radiation was measured by simply shading the diffuser with a "shading disc", from the direct solar beam. The target reflectance/radiance was measured by rotating the diffuser 180^{o} so that it viewed the target. The detailed calibration of the I.S.C.O instruments is given in the Appendix.

The second type of instrument used was a Bendix Model 100 Radiant Power Measuring Instrument (R.P.M.I.). This instrument was developed, by Dr. R. Rogers of the Bendix Aerospace Division, for ground calibration measurements for the Earth Resource Technology Satellite (ERTS). It was kindly supplied, at no cost. It is basically a filtered radiometer having bandpasses of (1) B1- .500 to .600 μm (micrometers), (2) B2- .600 to .700 μm, (3) .700 to .800 μm, and (4) .800 to 1.10 μm. Where the B1, B2, B3, and B4 are band No. 1, No. 2, etc; and they correspond to the ERTS bands 4,5,6, and 7. The real bands of the RPMI are (1) B1R - .505 to .590 μm, (2) .600 to .720 μm, (3) .680 to .815 μm, and (4) B4R - .810 to 1.02 μm. Both the ERTS and real bands are reported herein. The R.P.M.I. was used to derive atmospheric optical depth, and directional (nadar view) target reflectance (using standard reflectance cards) and absolute target radiance. All these were compared with the higher resolution ISCO derivations of same.

3.2 Measurements and Analyses

3.2.1 KATHERINE PLAYA, NEW MEXICO, 27 JAN. 1974

3.2.1.1 General Conditions - Poor. High winds causing intermittent dust clouds moving from north to south. Large cumulus clouds moving through area, causing shadows on the playa.

3.2.1.2 Near Surface Meteorology

3.2.1.3 Total and Diffuse Solar Radiation

3.2.1.4 Atmospheric Optical Depth/Transmittance

3.2.1.5 Target Reflectivity and Radiance at Ground Level

} Measurements either not reduced or not taken, due to poor conditions.

3.2.1.6 Target Radiance at EREP

3.2.2 GREAT SALT LAKE DESERT, UTAH, 29 JAN. 1974

3.2.2.1 General Conditions - Poor. High altitude cirrus cloud cover. Water standing on portions of the desert, remaining portions of desert were very muddy.

3.2.2.2 Near Surface Meteorology

3.2.2.3 Total and Diffuse Solar Radiation

3.2.2.4 Atmospheric Optical Depth/Transmittance

3.2.2.5 Target Reflectivity and Radiance at Ground Level

} Measurements either not reduced or taken, due to poor conditions

3.2.2.6 Target Radiance at EREP

3.2.3 KATHERINE PLAYA, NEW MEXICO, 01 FEB 1974

Site Coordinates:	$32^{\circ}18'00"$N Latitude $108^{\circ}53'00"$W Longitude (See Figure 11)
EREP Pass:	Track 06, Pass No. 98, Rev. 3798
Time of Overpass:	032:17:02:08 GMT 1102 MDT, Local

3.2.3.1 General Conditions - Clear

3.2.3.2 Near Surface Meteorology - Dry bulb temperature = 7.22°C; wet bulb temperature = 1.7°C; surface pressure = 662 mm of Hg (from U.S. Standard Atmosphere); wind - calm.

3.2.3.3 Total and Diffuse Solar Radiation - The absolute quantities of total and diffuse solar radiation are shown in Figures 14 and 15 respectively, and they are listed in Table 5 . The ratio of diffuse to total solar radiation is shown in Figure 16 , and is listed in table 5 .

3.2.3.4 Atmospheric Optical Depth/Transmittance Measurements - Measurements of the direct solar beam were made, over a period of time, in order to subsequently derive the optical depth of the atmosphere (τ). The optical depth of the atmosphere and the measurements of the direct solar beam (M) are related by Lambert's law, as follows.

$$M = M_o e^{-\tau m} \tag{1}$$

where M is the meter reading of the pyrheliometer (I.S.C.O or Bendix R.P.M.I., equipped with collimator), M_o is their extra-terrestrial meter reading, and m is the relative air mass. The relative air mass can be given as sec θ_o, where θ_o is the solar zenith angle, for air masses ≤ 2.0. For greater air masses, atmospheric refraction has to be taken into account. This was performed by using the following equation (which is a simplified version of Bemporad's formula).

$$C.F. = 5.534 \times 10^{-4} \sec \theta_o^{3.34} \tag{2}$$

and

$$m = \sec\theta_o - \left[C.F.\ p/p_o\right] \tag{3}$$

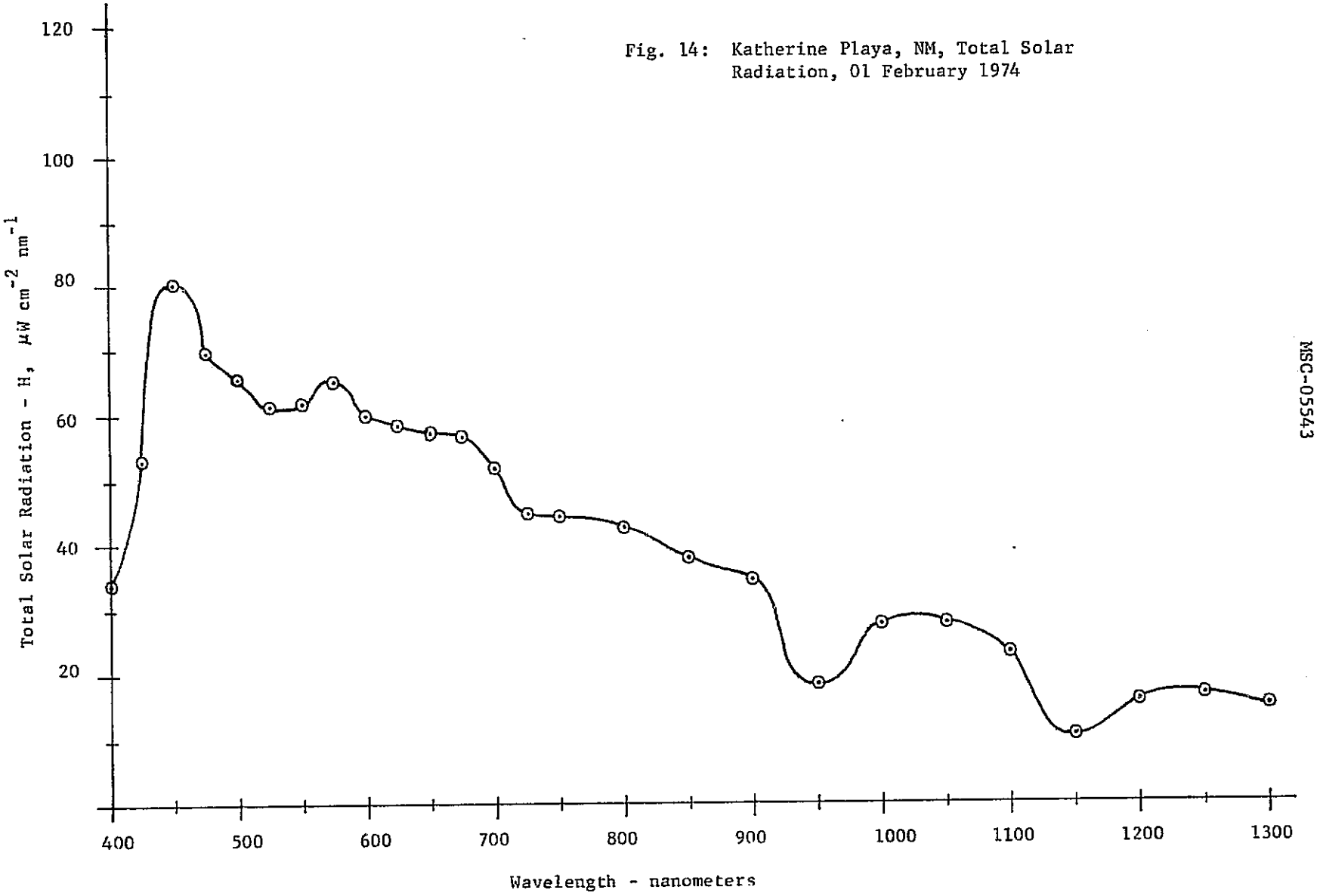

Fig. 14: Katherine Playa, NM, Total Solar Radiation, 01 February 1974

MSC-05543

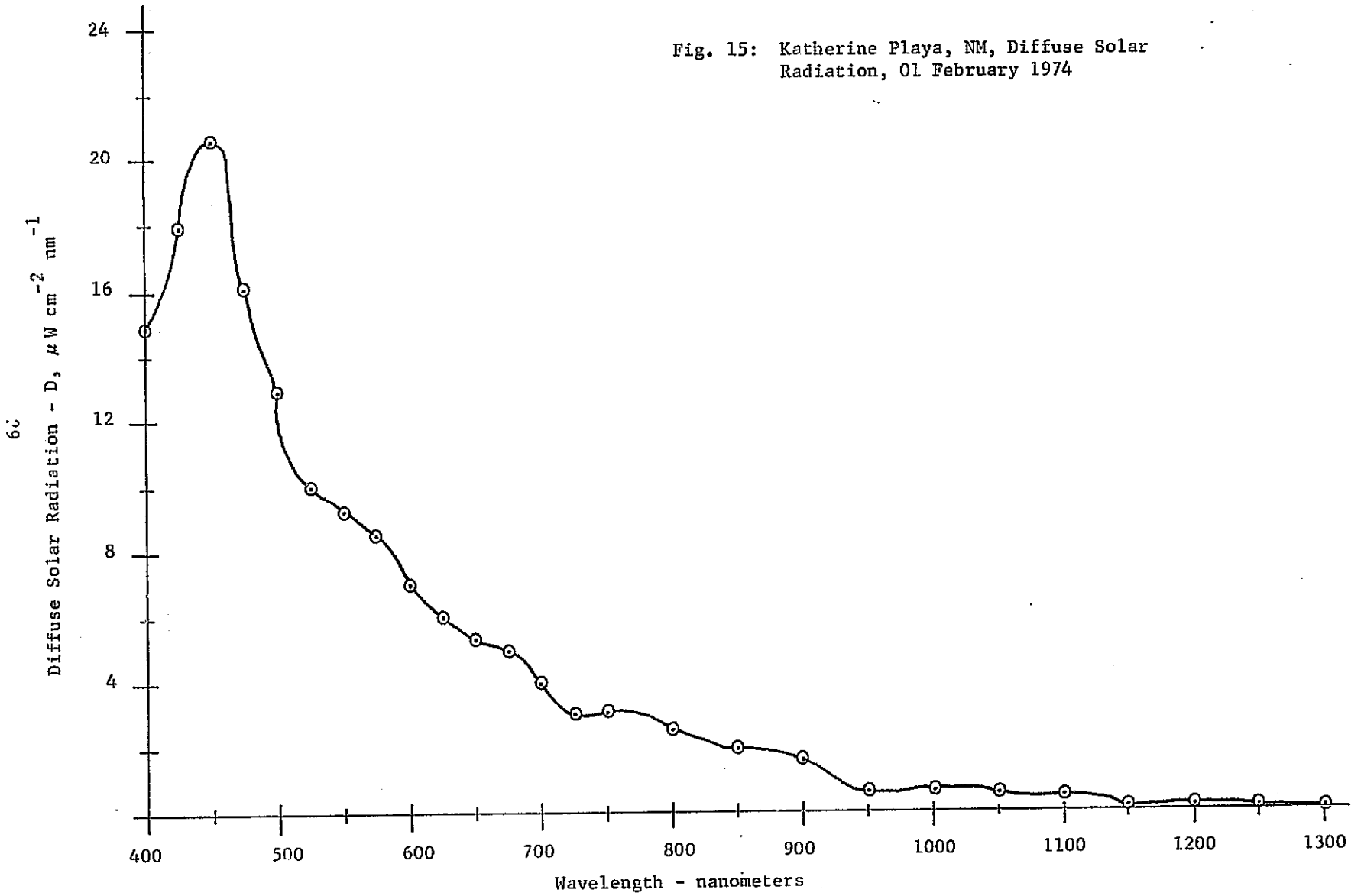

Fig. 15: Katherine Playa, NM, Diffuse Solar Radiation, 01 February 1974

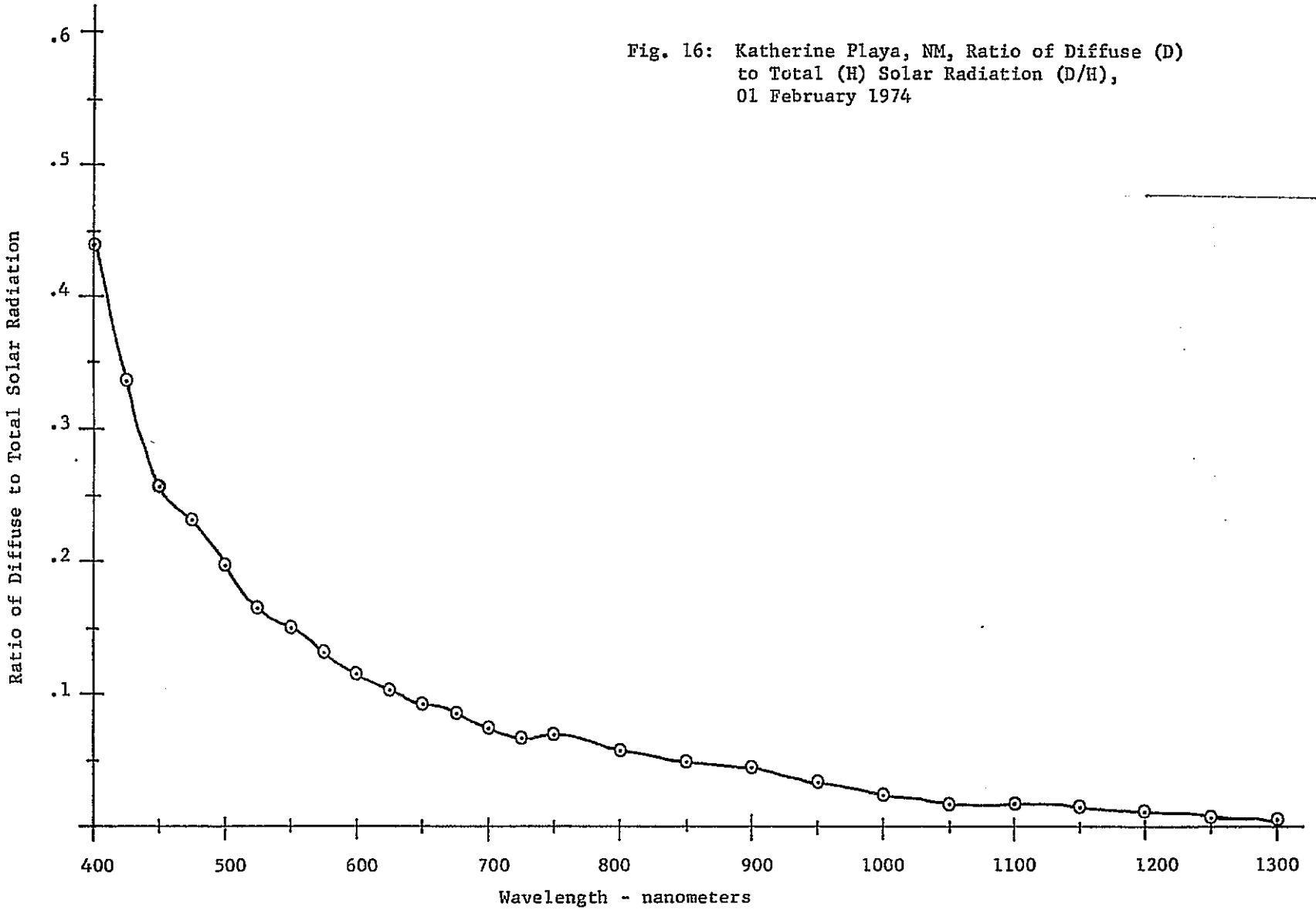

Fig. 16: Katherine Playa, NM, Ratio of Diffuse (D) to Total (H) Solar Radiation (D/H), 01 February 1974

KATHERINE PLAYA (02-01-74) TOTAL AND DIFFUSE SOLAR RADIATION

Wavelength (nm)	H (1036)*	D (1031)*	D/H
400	33.75	14.82	.439
425	53.24	17.84	.335
450	80.14	20.63	.257
475	69.43	16.07	.231
500	65.38	12.85	.197
525	61.28	10.08	.164
550	61.77	9.26	.150
575	65.20	8.58	.132
600	60.05	6.99	.116
625	58.44	6.04	.103
650	57.30	5.34	.093
675	56.94	4.88	.086
700	52.05	3.87	.074
725	44.83	3.05	.068
750	44.52	3.11	.070
800	42.46	2.48	.058
850	37.94	1.86	.049
900	34.58	1.61	.046
950	18.34	0.60	0.33
1000	27.69	0.66	.024
1050	27.66	.049	.018
1100	23.54	0.42	.018
1150	10.55	0.15	.014
1200	15.90	0.17	.011
1250	16.69	0.12	.007
1300	14.86	0.08	.005

* microWatts $(\text{centimeter})^{-2}$ $(\text{nanometer})^{-1}$, MDT.

Table 5: Katherine Playa, NM, Total and Diffuse Solar Radiation, 01 February 1974

where C.F. is the refraction correction factor, P is the atmospheric pressure at the site, and P_o is the pressure at sea level. In order to derive the optical depth, the pyrheliometer meter readings are plotted vs. air mass, as shown in Figures 17a to 17e. Extrapolation of the line yields M_o, and Equation 1 can then be solved to yield the optical depth. The degree of linearity of the plots is a direct indication of the degree of atmospheric stability, in terms of aerosol content, i.e.; the meter readings will deviate from a linear function if the atmospheric aerosol content varies as a function of time of day (air mass). As can be seen in Figures 17a to 17e the atmospheric conditions, above the Playa, were somewhat unstable. This is especially exhibited in the infrared region, where aerosols account for almost the entire optical depth. In cases of nonlinearities, an average had to be taken. This does result in some degree of uncertainty for the atmospheric transmittance ($T = e^{-\tau}$) for the radiance at EREP, as discussed later; because, EREP sensors viewed the target (nadir or near nadir) through an air mass of 1.0, i.e.; a nadir view is an angle of zero degrees and the air mass is given by the secant of the viewing angle. The resultant optical depths are shown in Figure 18. As can be seen, good agreement exists between the I.S.C.O and Bendix instruments. Shown also, is a model (Visual Range = 40 Km) derived from "Vertical Attenuation Model With Eight Surface Meteorological Ranges 2 to 13 Kilometers", L. Elternan, AFCRL - 70-0200, E.R.P. No. 318. This model, as discussed later, is then used to derive the atmospheric path radiance between the EREP sensors and the target. For detailed discussions of the relationship of optical depth to atmospheric aerosal, molecular, and water vapor current, a paper entitled, "Spectral Distribution of Solar Radiation at the Earth's Surface",

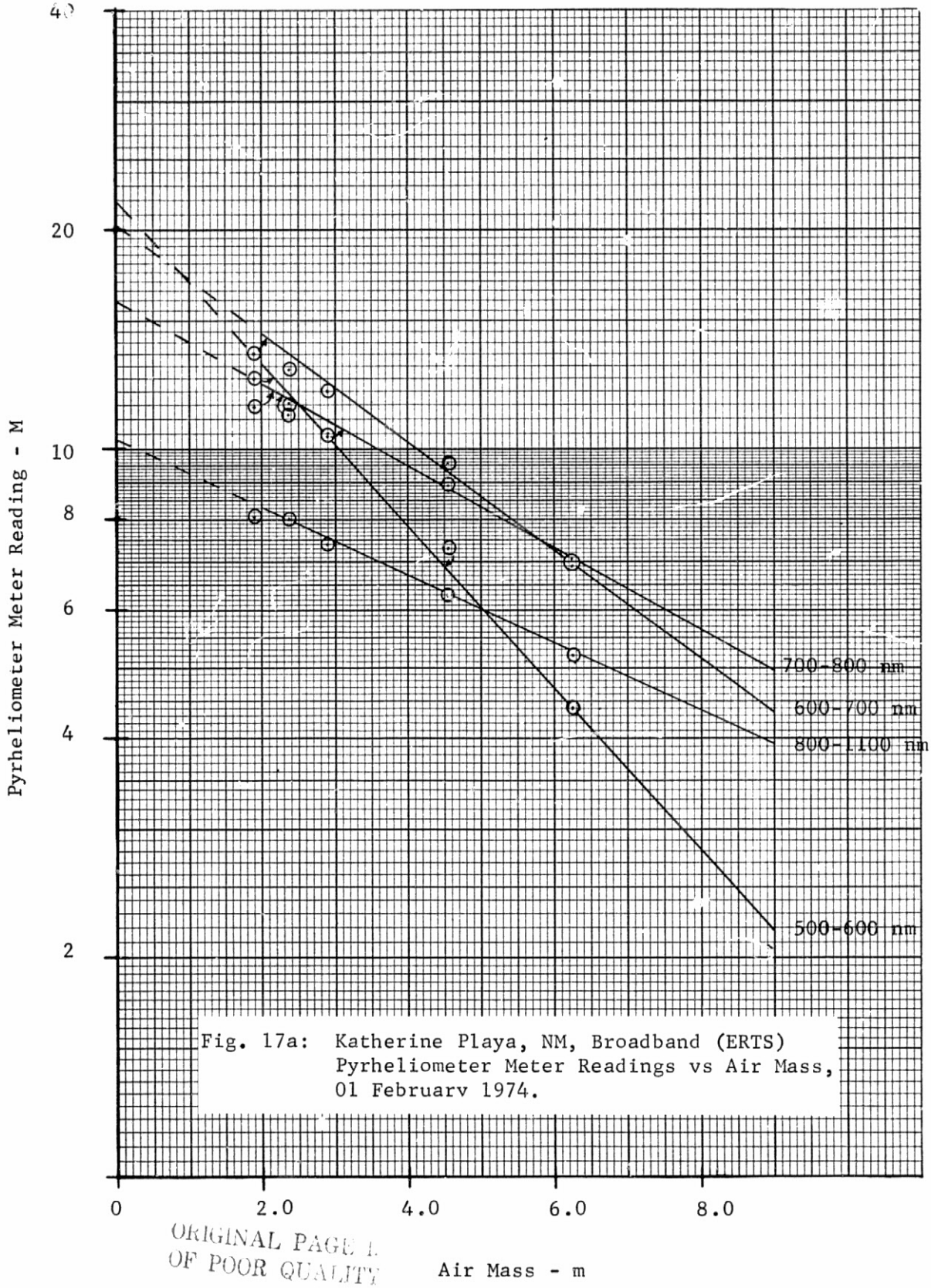

Fig. 17a: Katherine Playa, NM, Broadband (ERTS) Pyrheliometer Meter Readings vs Air Mass, 01 Februarv 1974.

Fig. 17b: Katherine Playa, NM, Spectral Pyrheliometer Meter Readings vs Air Mass, 01 February 1974

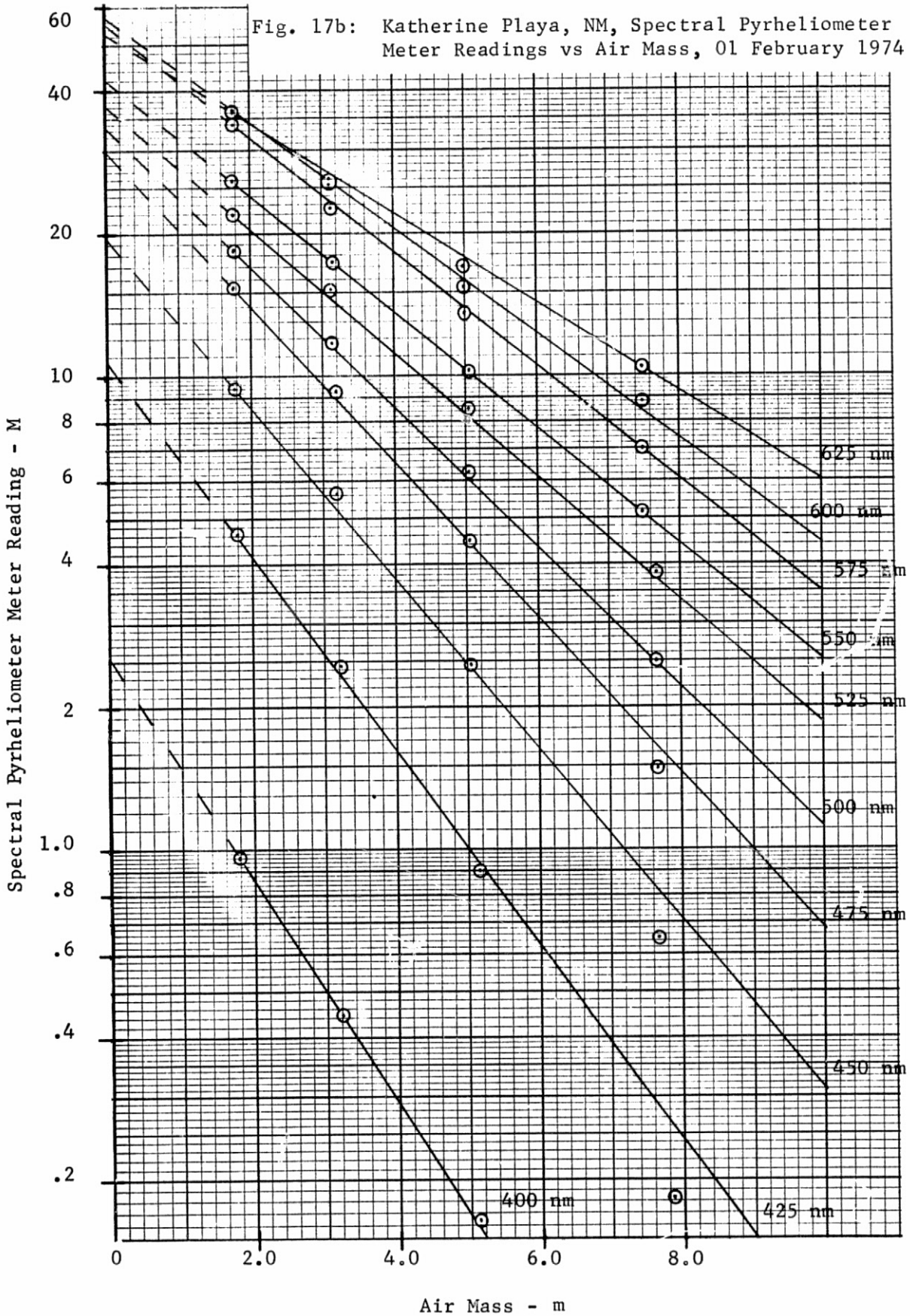

Fig. 17c: Katherine Playa, NM, Spectral Pyrheliometer Meter Readings vs Air Mass, 01 February 1974

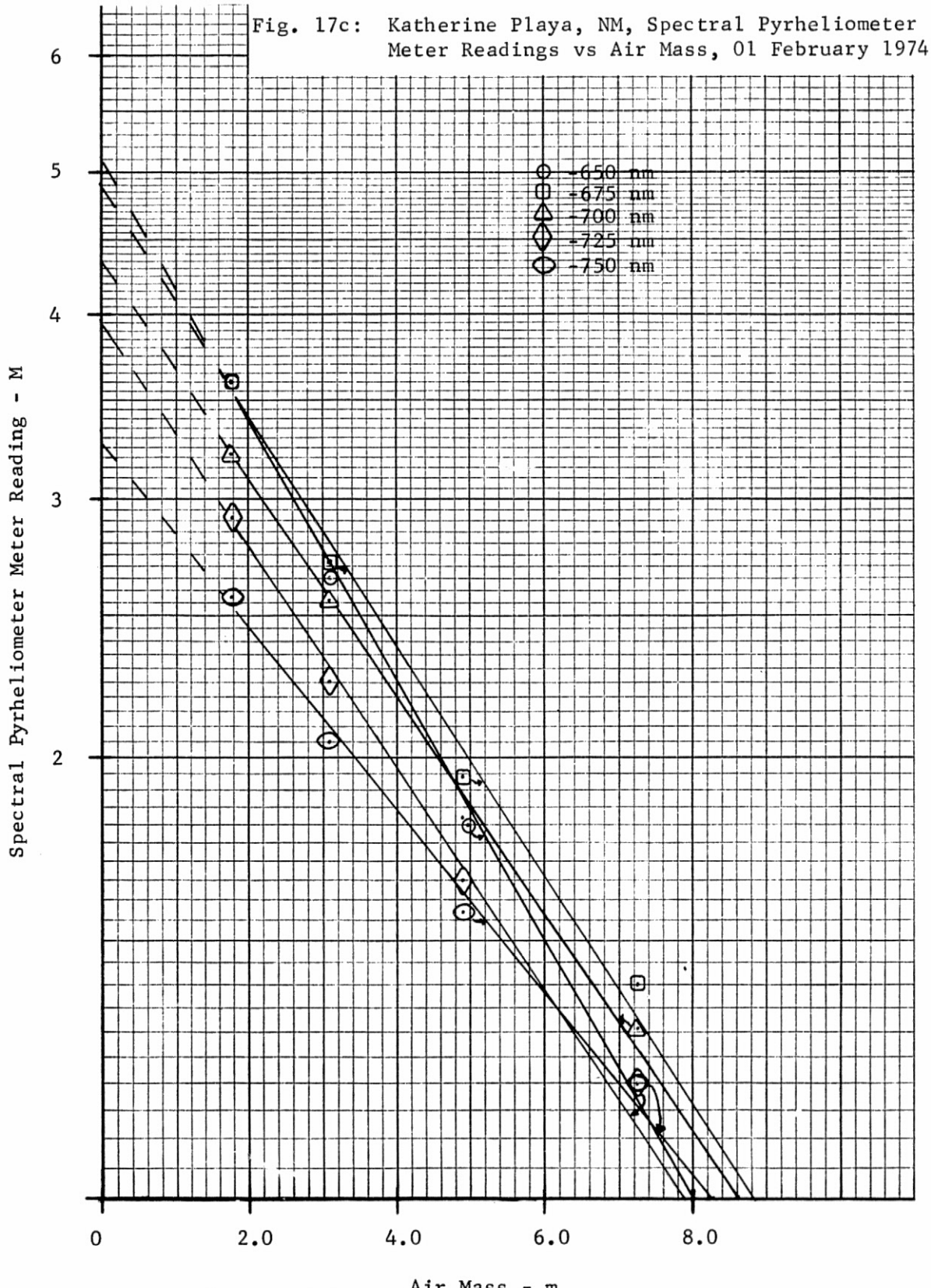

Fig. 17d: Katherine Playa, NM, Spectral Pyrheliometer Meter Readings vs Air Mass, 01 February 1974

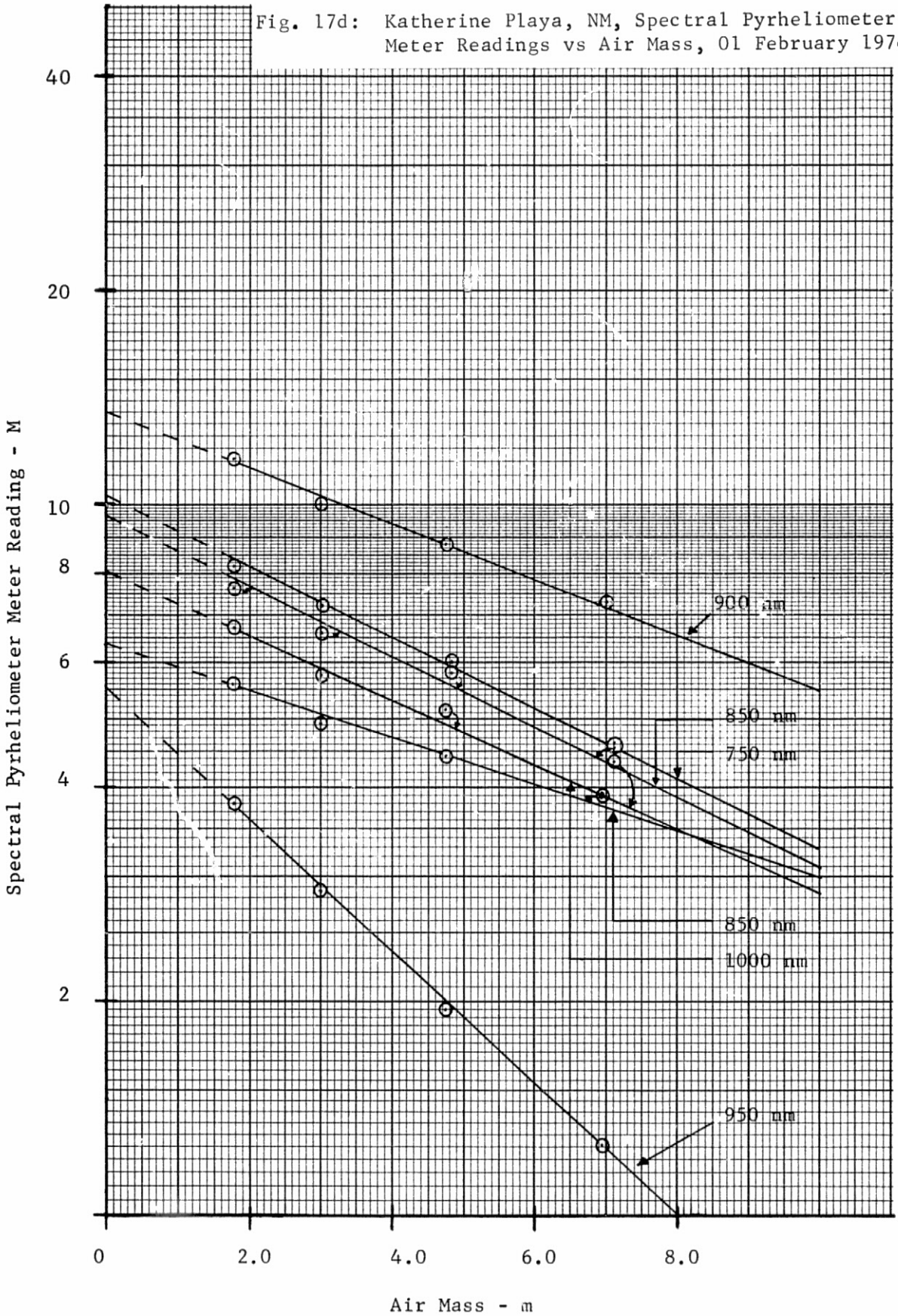

Fig. 17e: Katherine Playa, NM, Spectral Pyrheliometer Meter Readings vs Air Mass, 01 February 1974

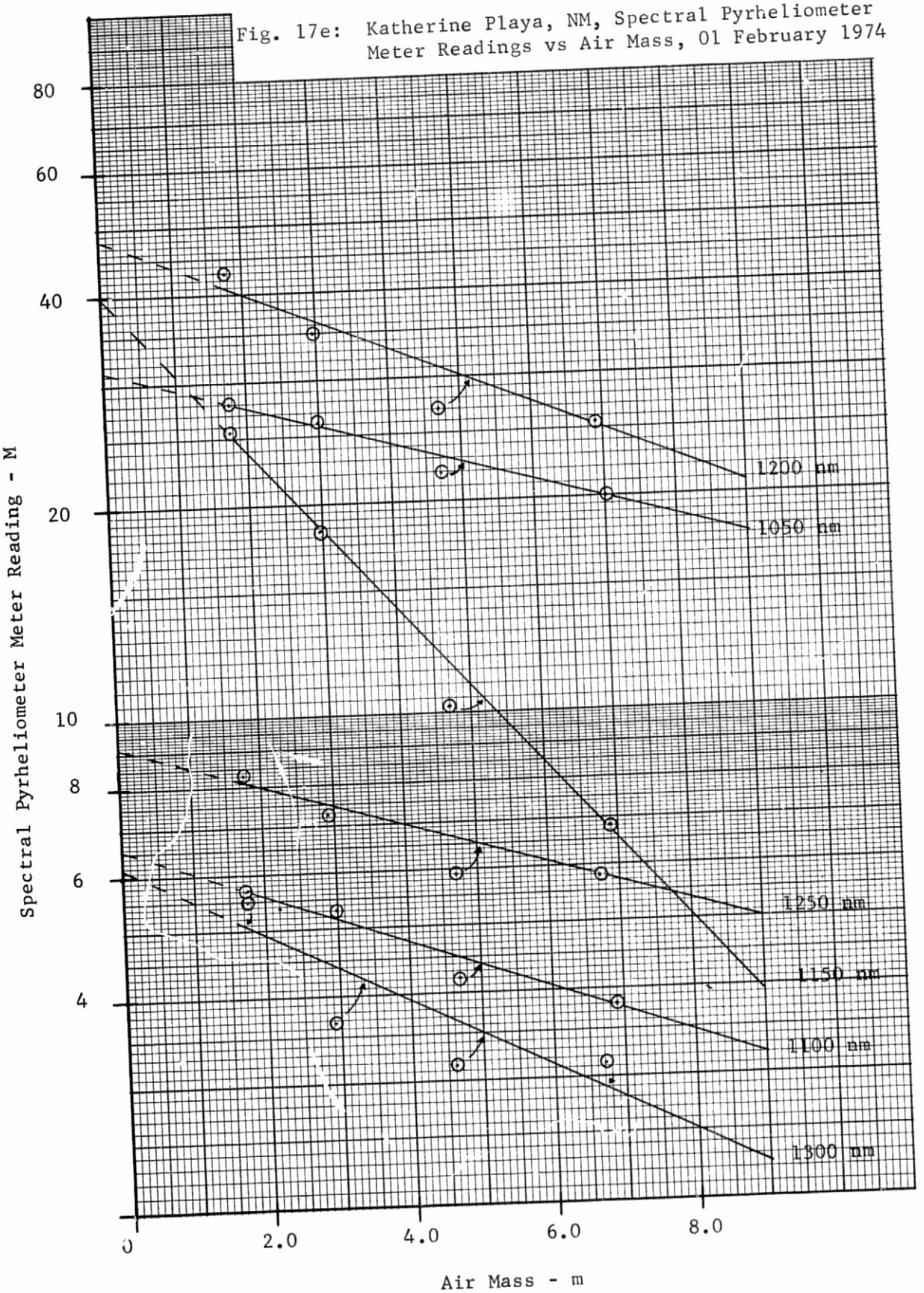

Fig. 18: Katherine Playa, NM, Broadband, Spectral and Model Optical Depth, 01 February 1974

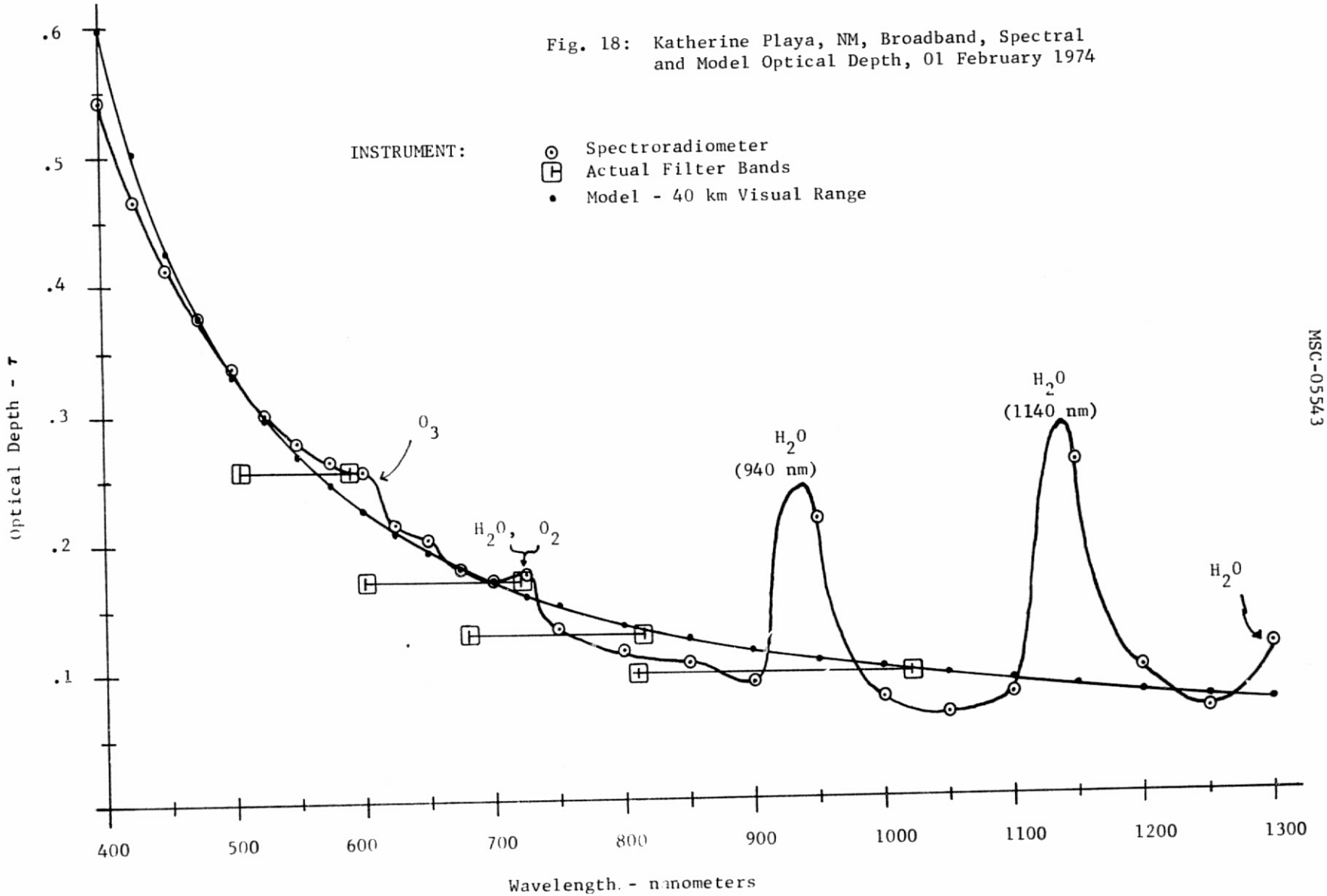

MSC-05543

D. M. Gates, Science, Vol. 151, No. 3710, 4 Feb. 1966, can be consulted.

3.2.3.5 Target Reflectivity and Radiance at Ground Level - Kathrine Playa is a typical dry lake bed mud flat, having a fair degree of uniformity. The target surface consists of polygon shaped, dried mud features (about 2 to 6 inches across) surrounded by a shallow crevice, containing a higher "albedo", fine grain "dust" material.

Both spectral (ISCO) and broadband (Bendix R.P.M.I.) measurements of target reflectivity and radiance were made, at the main site shown in Figure 22. As discussed previously, the I.S.C.O. reflectivity measurements were made by measuring the total incoming solar radiation, then rotating (180°) the diffuser/fiber optics probe so that it viewed the target, then taking a ratio (reflectivity) of the outgoing to incoming radiation. The directional, (nadir view), Bendix R.P.M.I. measurements were made by first viewing a standard "gray" card ,then the target, then a standard "white" card; the targets reflectivity was then determined by comparing the radiances (meter readings) of the standard cards vs. the target, shown in Figure 20. The results are shown in Figure 21. As can be seen good agreement exists between the I.S.C.O. and Bendix R.P.M.I. determinations. Also, it can be seen that the targets reflectivity varied as a function of sun angle (time); this is probably due to the extremely low sun angles due to the time of the year (winter).

In order to determine the reflectivity nature of the entire playa, the Bendix R.P.M.I. was mounted to the under carriage of a helicopter, and flown on flight paths shown in Figure 22. Due to operator time limitations, a complete set of band (B1, B2, B3, and B4) measurements could only be made at three posi-

tions, see Figure 22. Target radiance for band No. 2 (.6 to .7 μm) was measured at twelve other positions on the playa. The results are listed in Table 6 ; plus, a comparison with the main site. The values listed in Table 6 have been corrected for collimator radiance and normalized to EREP overpass. This was performed by using premission and postmission measurements of the standard "white" card radiances; plus, real time (during the helicopter flight) measurements of total incident (.4 to 1.1 μm) solar radiation were made and radioed to the operator in the helicopter. He then recorded them according to the corresponding Bendix R.P.M.I. radiance measurements. The target radiance at EREP overpass (1102 MDT) is related (normalized) to the target radiance measured from the helicopter, at some other time (t) by

$$N_{\text{EREP}}(1102) = N_{\text{Helicopter}}(t) \times \frac{H(1102)}{H(t)} \qquad (4)$$

where H(1102) is the broadband (.4 to 1.1 μm) measurement of total incoming radiation at 1102 (EREP overpass), and H(t) is the corresponding measurement during the helicopter mission. As mentioned previously, the radiances of standard "gray" and "white" cards were also used to normalize the helicopter data to EREP overpass. Instead of the normalization factor of H(1102)/H(t) a factor of $N_W(1102)/N_W(t)$ was used, where N_W is the "white" card radiance at the EREP overpass (1102) and during the helicopter mission $N_W(t)$. The "white" card radiance during the helicopter mission was derived (interpolated with respect to time) from pre and post flight measurements. The use of the "white" card measurements allowed normalization factors to be derived for each wavelength band, as apposed to the broadband (.4 to 1.1 μm) total measurements. The two methods of deriving the

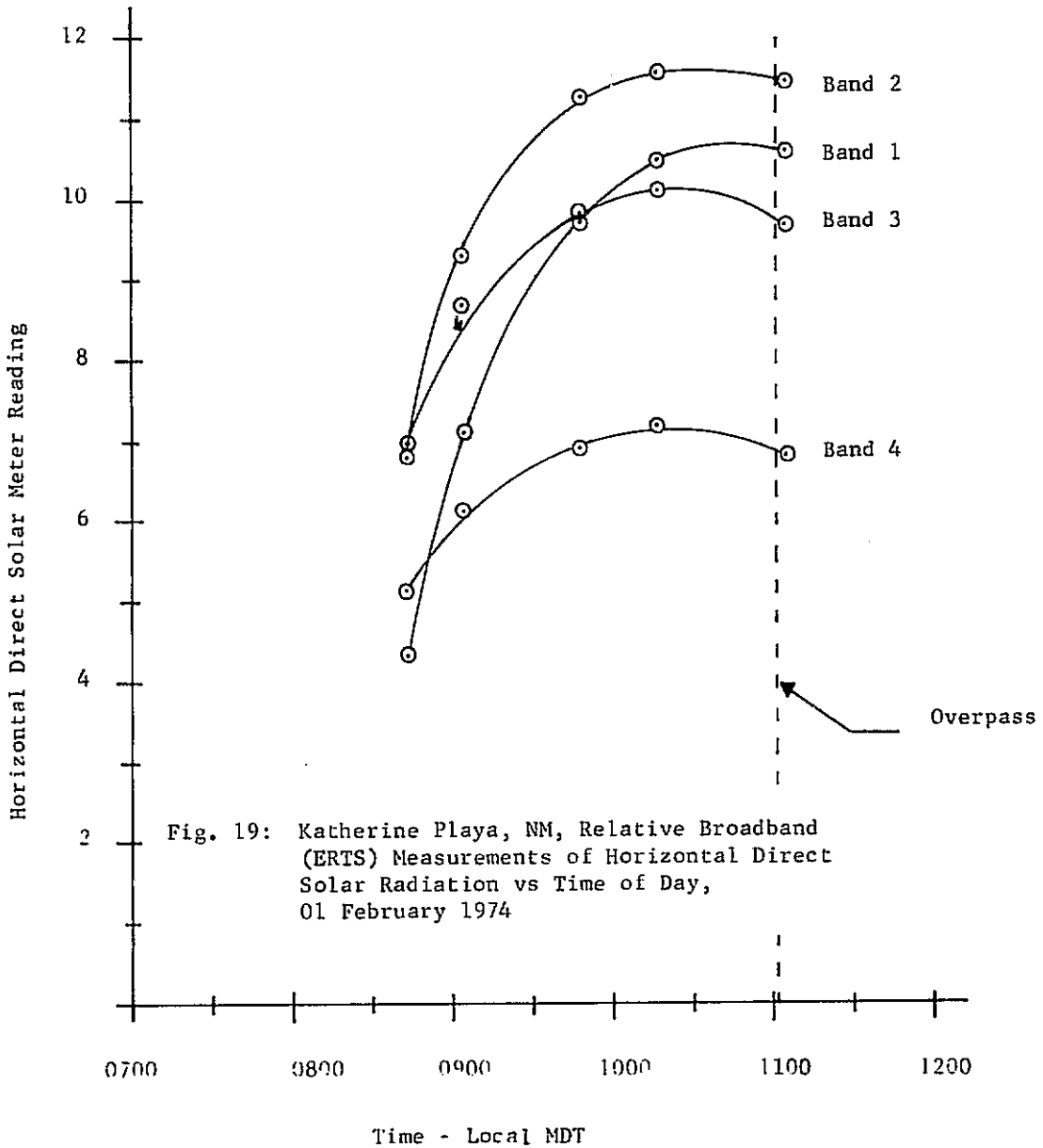

Fig. 19: Katherine Playa, NM, Relative Broadband (ERTS) Measurements of Horizontal Direct Solar Radiation vs Time of Day, 01 February 1974

Fig. 20: Katherine Playa, NM, Determination of Target Reflectivity using Cards, 01 February 1974, (1058 MDT)

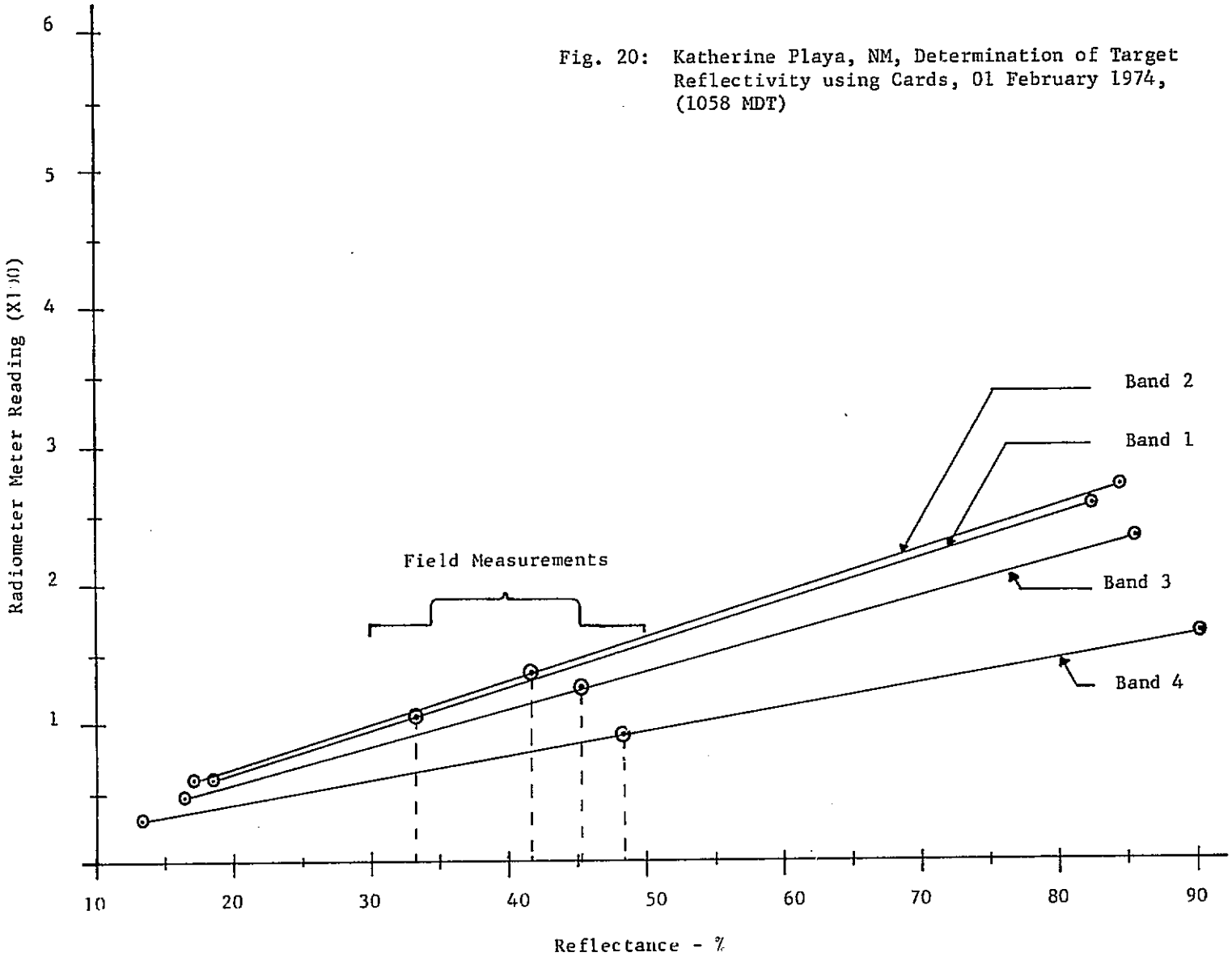

Fig. 21: Katherine Playa, NM, Broadband (ERTS) and Spectral Target Reflectivities, 01 February 1974

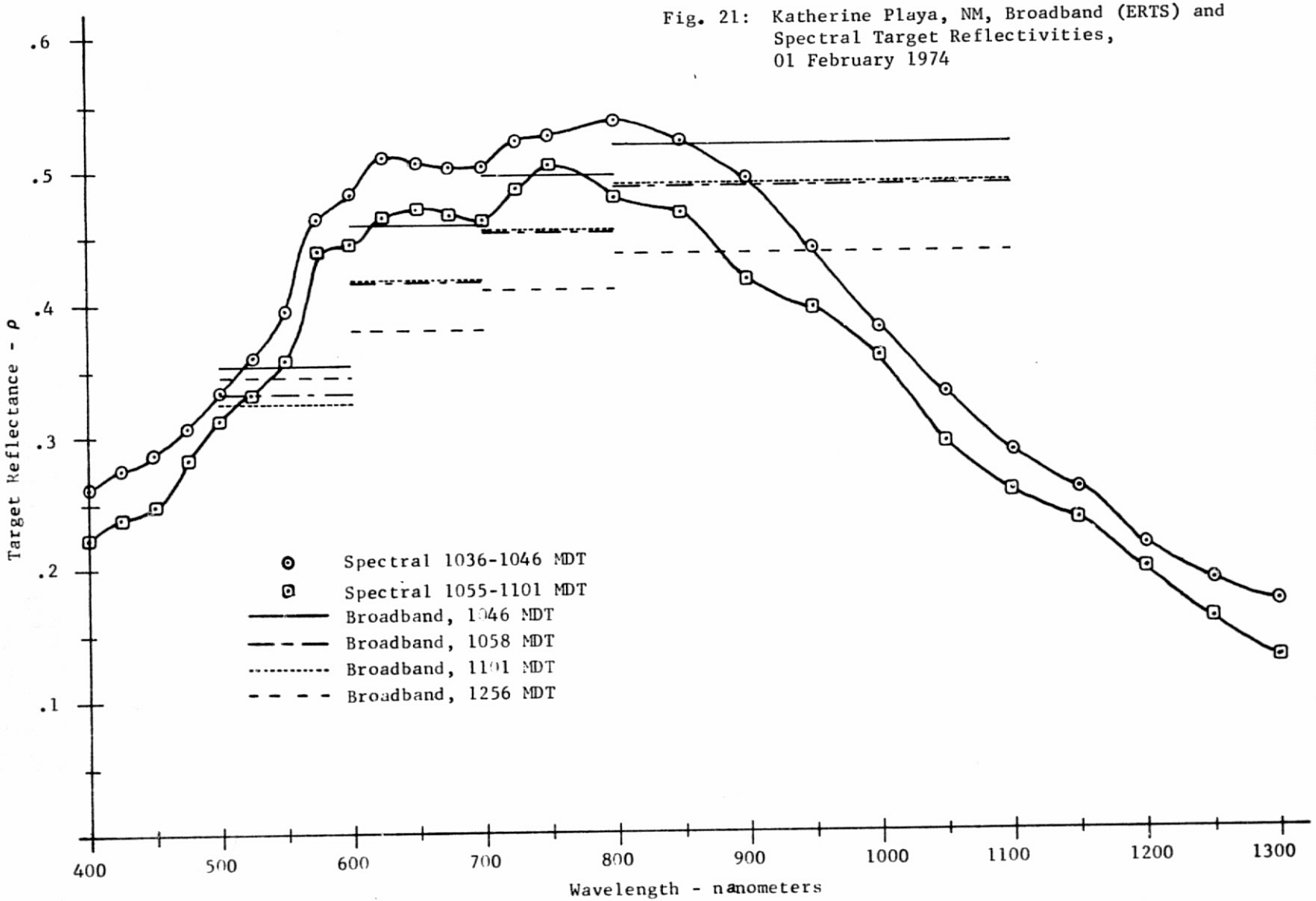

MSC-05543

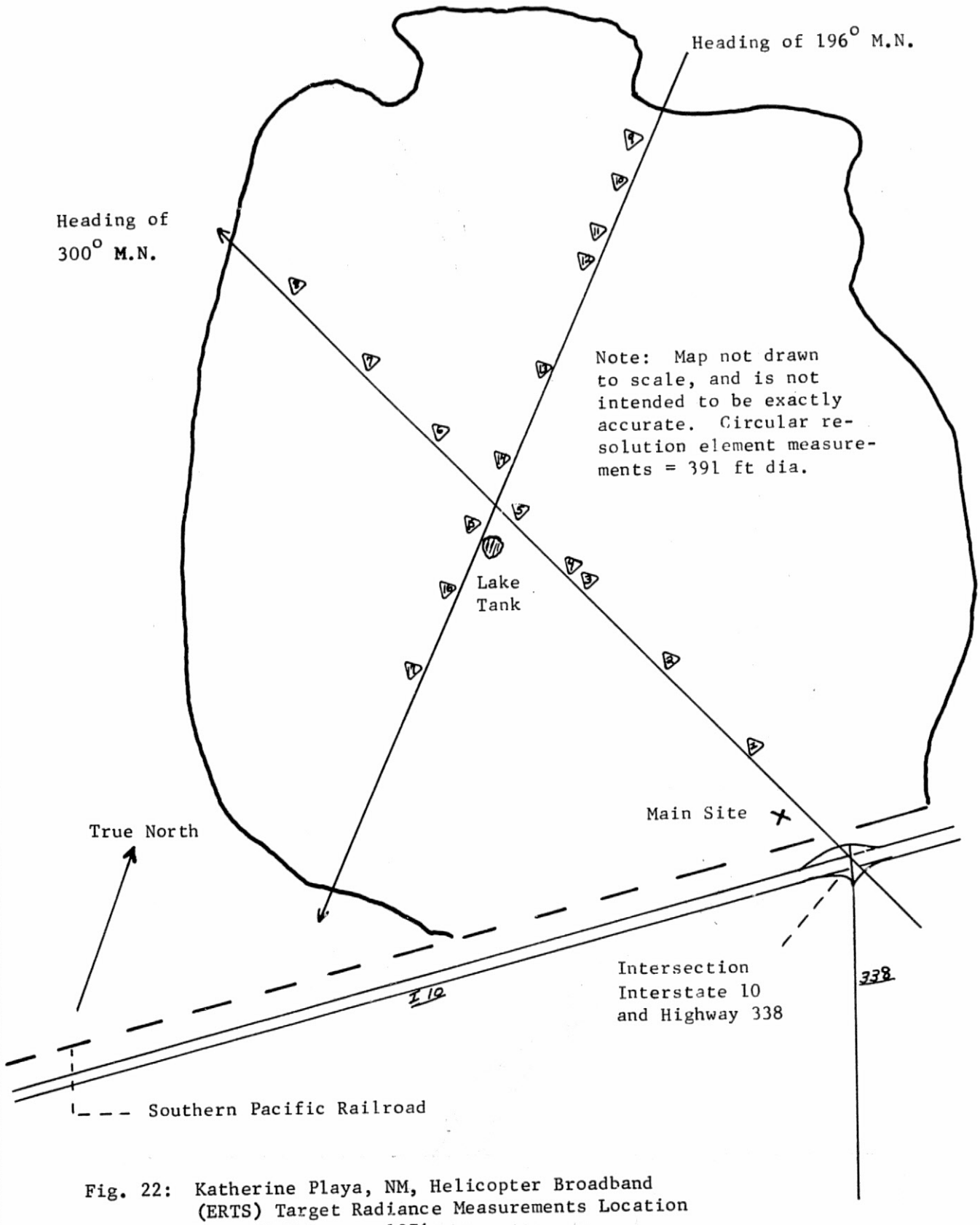

Fig. 22: Katherine Playa, NM, Helicopter Broadband (ERTS) Target Radiance Measurements Location Map, 01 February 1974

HELICOPTER TARGET RADIANCE MEASUREMENTS*

Position	B1	B2	B3	B4
1		10.65		
2	9.20	9.91	8.94	17.62
3		9.83		
4		9.49		
5		9.98		
6		11.06		
7		10.52		
8		9.98		
9		5.59		
10		8.20		
11		7.88		
12	7.67	8.26	7.39	15.22
13		8.74		
14		9.73		
15		10.78		
16		9.99		
17	9.35	9.91	9.14	17.86
Mean	8.74	9.44	8.49	16.90
Main Site	8.39	9.42	8.85	19.31

* Katherine Playa, New Mexico, 01 Feb. 1974, W m^{-2} $\Delta\lambda^{-1}$ sr^{-1}

B1 - .500 to .600 μm

B2 - .600 to .700 μm

B3 - .700 to .800 μm

B4 - .800 to 1.100 μm

Table 6: Katherine Playa, NM, Helicopter Broadband (ERTS) Target Radiance Measurements, 01 February 1974

target radiance at EREP overpass resulted in very consistent results (2-3%); thereby resulting in a high degree of certainty. A comparison given in Table 5 , of all the helicopter measurements (their mean) with the main site measurements, shows that the main site was fairly typical of the playa. However, sites existed on the playa that were significantly higher and lower in reflectivity; with the lower reflectivity sites existing near the edges of the playa and the higher reflectivity sites existing near the center of the playa.

3.2.3.6 Target Radiance at EREP - The apparent target radiance at the EREP sensors, N_s, is the sum of the directional target radiance (that reflected from the target), $N_t(d)$, and radiance introduced (backscattered) by the intervening atmospheric column of aerosols and molecules, N_a. Hence,

$$N_s = N_t(d) + N_a \tag{5}$$

where $N_t(d)$ can further be given as

$$N_t(d) = \frac{\rho H T}{\pi} \tag{6}$$

where ρ is the target reflectivity, H is the total incident solar radiation, and T is the atmospheric transmittance - given as $T = e^{-\tau \sec\theta}$. Where θ is the sensor view angle (scan angle) and τ is the previously discussed optical depth. The total solar radiation is equal to the sum of the direct (on a horizontal surface), I_h, and the global diffuse radiation, S, hence

$$H = I_h + S \tag{7}$$

The direct solar radiation can be given as

$$I_h = I_o \cos \theta_o \, e^{-\tau \sec \theta_o} \qquad (8)$$

where I_o is the extraterrestrial solar constant, and θ_o is the solar zenith angle.

The directional target radiance, $N_t(d)$, is derived from all measured quantities - ρ, H, and T ($e^{-\tau \sec \theta}$). The atmospheric path radiance, N_a, between the EREP sensors and the target can not be measured directly. In order to determine N_a, a radiative transfer computer program* was employed. This program was modified to allow it to be used on the CDC 6000 MACE Operating System, at Martin Marietta Aerospace, Denver Division. The required program inputs (path radiance determinates) are (1) altitude of sensor, (2) target reflectivity, (3) target background reflectivity, (4) solar zenith angle, (5) solar-sensor azimuth angle, (6) sensor scan angle (view angle), and (7) atmospheric visual range. The altitude of the sensor was input as 50 Km, which is equivalent to orbital altitude. The target reflectivity was a measured input; the target's background albedo was taken to be equivalent to the targets reflectivity. For the area, Katherine Playa, under consideration this assumption is reasonable. Solar zenith and solar-sensor azimuth angles were available from SKYBET data, and ephemeris data. The sensor scan angle was varied from 0 to 5^o. The atmospheric visual range is defined as that distance an object, having a 2% contrast with the sky background, can be seen. Such a measurement is difficult (often impossible) to make. Instead, the measured atmospheric optical depth was used to select a visual range model that yielded a close fit between the measured and model optical

* "Studies of Spectral Discrimination", W. A. Malila, et. al., Report No. NAS CR-WRL31650-22-T, Contract No. NAS9-9784, May 1971.

depth. As can be seen in Figure 18, this technique was successful. The field measurement derived visual range was then input into the program, and the atmospheric path radiance calculated. The resultant target radiances and path radiances at EREP are shown in Figures 23 and 24, and are listed in Tables 7, 8, and 9.

A discussion of the errors associated with the above techniques of deriving path radiance and radiance at EREP is given in the Appendix.

Fig. 23: Katherine Playa, NM, Broadband (ERTS) and Spectral Target Radiance at Ground Level, 01 February 1974

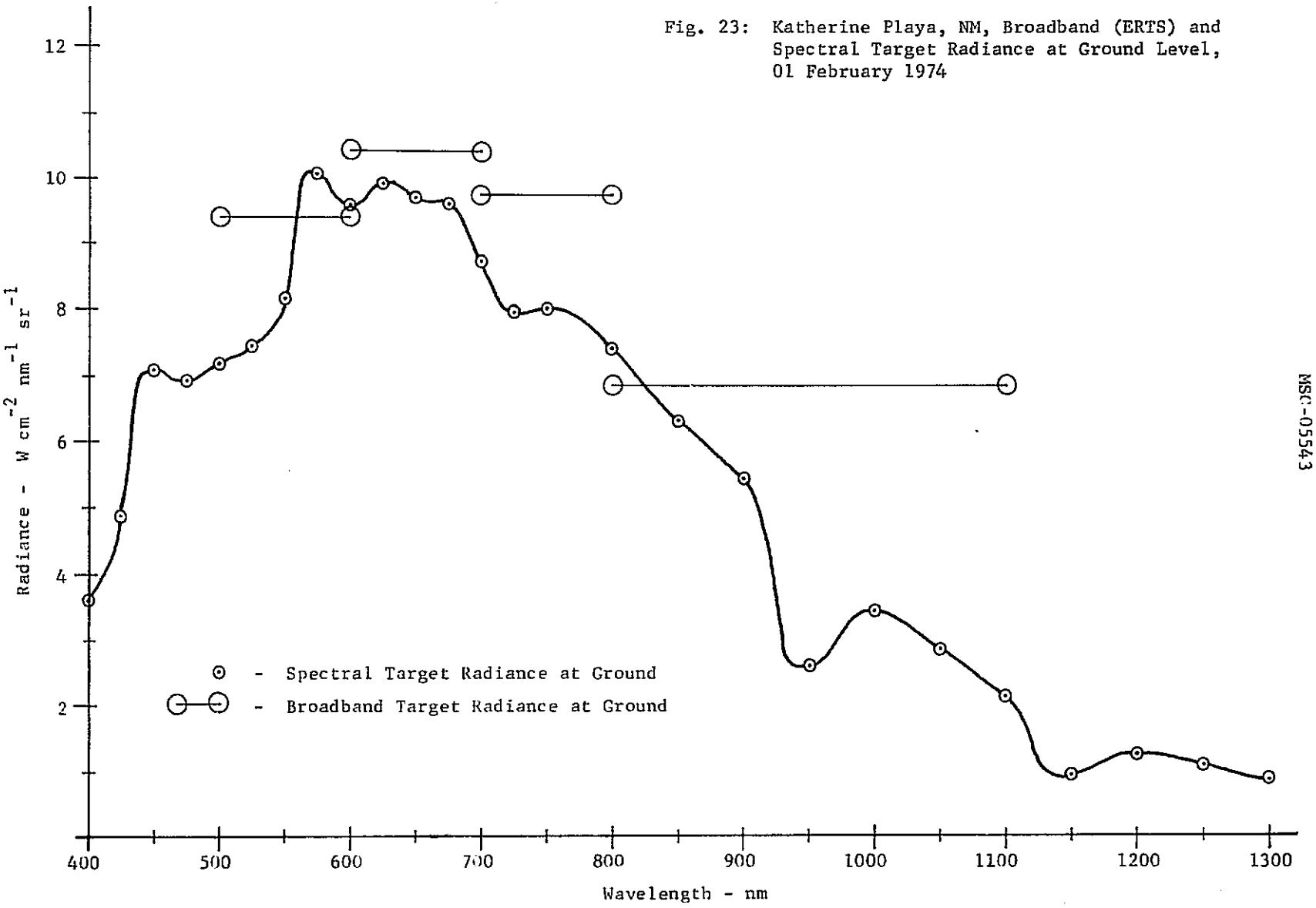

MSC-05543

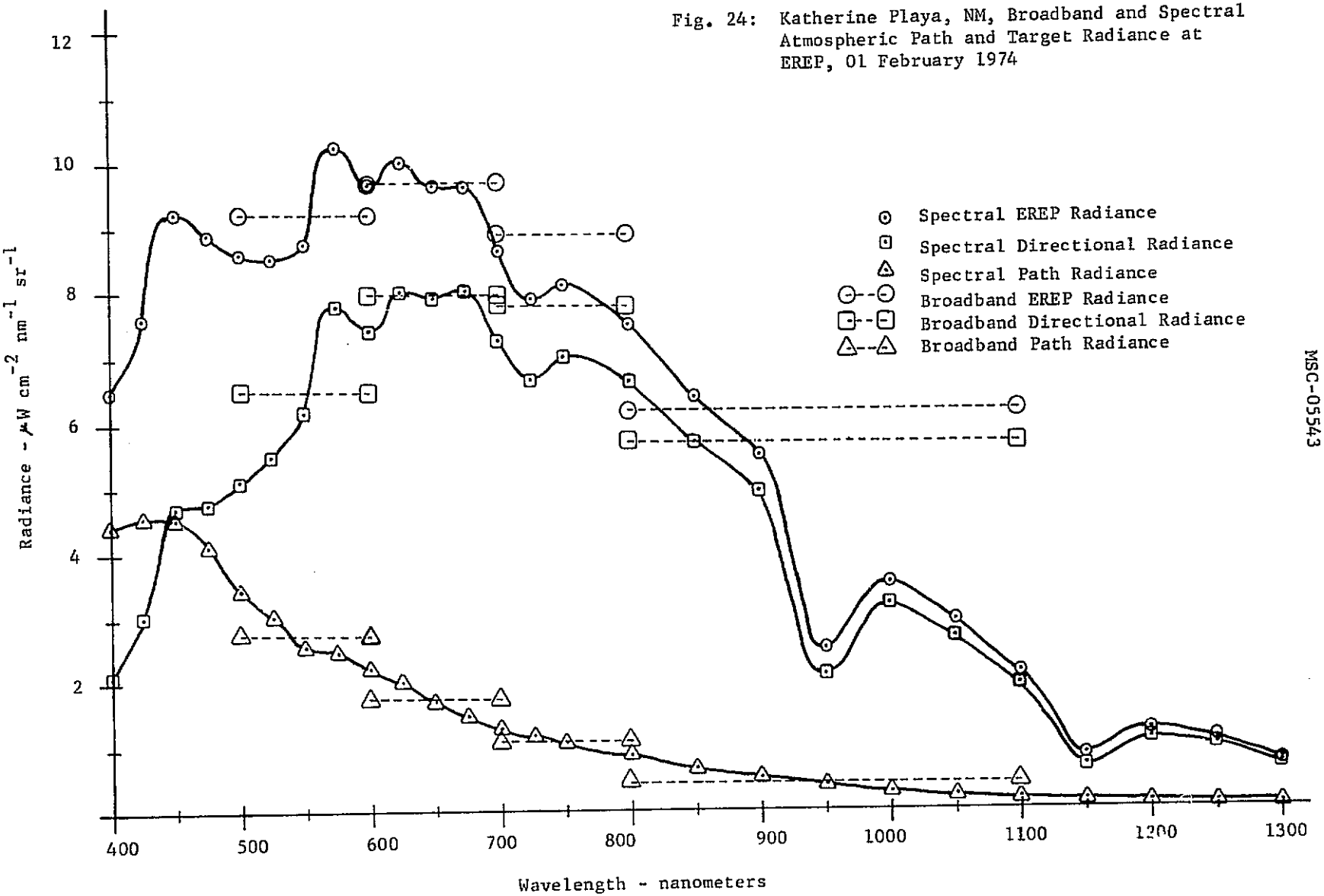

Fig. 24: Katherine Playa, NM, Broadband and Spectral Atmospheric Path and Target Radiance at EREP, 01 February 1974

MSC-05543

Katherine Playa (02/01/74) Broadband Target Radiance at Ground

Band	Meter	Correction Factor	$N_t(g)_{Meas}$	Collimeter Correction	$N_t(g)_{Corr}$*
B1	.0105	895	9.40	1.12	8.39
B1R		743	7.80	1.12	6.96
B2	.0138	758	10.46	1.11	9.42
B2R		943	13.01	1.11	11.72
B3	.0126	773	9.74	1.10	8.85
B3R		1079	13.60	1.13	12.04
B4	.0092	2245	20.66	1.07	19.31
B4R		1665	15.32	1.12	13.68

* $\left\{ \begin{array}{l} N_t(g) \div \text{Collimator Correction} \\ \text{Watts (meter)}^{-2} \text{ (steradian)}^{-1} \ \Delta\lambda^{-1} \end{array} \right.$

$\Delta\lambda$ (micrometer) = B1 = .500 - .600 B1R = .505 - .590
B2 = .600 - .700 B2R = .600 - .720
B3 = .700 - .800 B3R = .680 - .815
B4 = .800 - 1.100 B4R = .810 - 1.022

Table 7: Katherine Playa, NM, Broadband Target Radiance at Ground, 01 February 1974

Katherine Playa (02-01-74) Broadband Atmosphere and Target Radiance							
Band	τ	T	Reflectance (ρ)	$N_t(g)^*$	$N_t(d)^*$	N_a^*	N_s^*
B1	.255	.774	.333	8.39	6.49	2.73	9.22
B2	.170	.844	.417	9.42	7.95	1.76	9.71
B3	.128	.880	.453	8.85	7.79	1.09	8.88
B4	.107	.889	.487	19.41	17.26	1.36	18.62

* Watts (meter)$^{-2}$ (steradian)$^{-1}$ $\Delta\lambda^{-1}$ [Incorporates Collimator Radiance Correction]

$\Delta\lambda$ (micrometer) = B1 = .500 - .600
B2 = .600 - .700
B3 = .700 - .800
B4 = .800 - 1.100

τ = Atmospheric Depth
T = Transmittance = $e^{-\tau \sec\theta}$

$N_t(g)$ = Target Radiance at Ground Level = $N_{(t)}g(meas)$

$N_t(d)$ = Target Directional Radiance at EREP = $[N_{(t)}g]$ T

N_a = Atmospheric Path Radiance

N_s = Radiance at EREP = $N_{(t)}d + N_a$

Table 8: Katherine Playa, NM, Broadband (ERTS)
Atmospheric and Target Radiance,
01 February 1974

KATHERINE PLAYA (02-01-74) SPECTRAL ATMOSPHERIC AND TARGET RADIANCE

Wavelength (nm)	τ	T	H(1102 MDT)**	ρ	$N_t(g)$***	$N_t(d)$***	N_a***	N_s***
400	.541	.582	51.5	.222	3.642	2.120	4.401	6.521
425	.465	.628	64.454	.238	4.974	3.061	4.551	7.612
450	.412	.662	90.206	.248	7.133	4.722	4.533	9.255
475	.376	.687	77.001	.283	6.940	4.768	4.128	8.896
500	.338	.713	72.184	.313	7.195	5.130	3.454	8.584
525	.300	.741	70.369	.332	7.444	5.516	3.022	8.538
550	.278	.757	71.357	.359	8.155	6.173	2.572	8.745
575	.262	.770	71.951	.440	10.072	7.755	2.498	10.253
600	.255	.775	67.755	.445	9.587	7.430	2.237	9.667
625	.214	.807	67.102	.465	9.927	8.011	2.016	10.027
650	.202	.817	64.720	.471	9.698	7.923	1.737	9.660
675	.180	.835	64.684	.457	9.621	8.033	1.520	9.553
700	.177	.838	59.182	.463	8.729	7.314	1.328	8.642
725	.174	.840	51.240	.487	7.949	6.678	1.215	7.893
750	.132	.876	49.736	.506	8.015	7.021	1.087	8.108
800	.116	.890	48.871	.479	7.453	6.633	.865	7.498
850	.105	.900	42.721	.468	6.348	5.722	.681	6.403
900	.091	.913	40.962	.417	5.432	4.959	.529	5.488
950	.216	.806	20.674	.396	2.603	2.098	.424	2.522
1000	.077	.926	30.275	.360	3.467	3.211	.318	3.529
1050	.065	.937	30.618	.294	2.869	2.688	.238	2.926
1100	.079	.924	25.849	.258	2.123	1.961	.178	2.139
1150	.258	.773	12.334	.235	0.923	0.713	.140	0.853
1200	.098	.907	19.713	.240	1.245	1.129	.104	1.233
1250	.109	.897	21.837	.159	1.103	0.989	.081	1.070
1300	.191	.826	20.209	.129	0.831	0.686	.066	0.752

** microWatts (centimeter)$^{-2}$ (nanometer)$^{-1}$

*** microWatts (centimeter)$^{-2}$ (nanometer)$^{-1}$ (steradian)$^{-1}$

τ = Atmospheric Depth

T = Transmittance = $e^{-\tau \sec\theta}$

H = Total Solar Radiation

ρ = Reflectance

$N_t(g)$ = Target Radiance at Ground Level = $\frac{\rho H}{\pi}$

$N_t(d)$ = Target Directional Radiance at EREP = $\left[N_t(g)\right]$ T

N_a = Atmospheric Path Radiance

N_s = Radiance at EREP = $N_t(d) + N_a$

Table 9: Katherine Playa, NM, Spectral Atmospheric and Target Radiance, 01 February 1974

APPENDIX

Instrument Calibrations, Analyses
Techniques, and Error Analyses

1. NEAR SURFACE METEOROLOGY

The near surface meteorology measurements were made with a sling psychrometer, dry and wet bulb temperatures - accuracy of $\pm$ 1°F; a hand-held cup anemometer - accuracy of $\pm$ 2 m.p.h., and an aneroid barometer - accuracy of $\pm$ .1 in. of Hg.

2. ATMOSPHERIC TEMPERATURE AND HUMIDITY PROFILES

The atmospheric temperature and humidity profiles were obtained by releasing a Colspan Environmental Systems Co. (Boulder, CO) radiosonde from a helicopter. Data from a coated bead thermistor (temperature) and a carbon element hygristor (ML-476) were telemetered to a ground receiving station (403 MHZ). The radiosonde descended to the surface on a parachute at approximately 25-26 ft/sec. The data was recorded on two identical strip charts, during the radiosonde descent. To calibrate the radiosonde temperature sensor/recorder, an internal potentiometer (within the ground station) is set just prior to being loaded into the helicopter. This potentiometer adjusts the slope of the current vs. temperature response, which is set according to the measured (mercury thermometer) ambient air temperature. Because the current output of the sensor is linear with respect to temperature, the atmospheric profile temperatures can then be accurately determined, based on the ground-based mercury thermometer calibration. To calibrate the humidity sensor, just prior to being loaded in the helicopter, the hygristor is replaced with a precise 20k ohm resistor. This value of resistance corresponds to a humidity of 33%, an internal potentiometer is then set to correspond to this humidity. Calibration tables relating the outputs of the bead thermistor and hygristor sensors to temperature and humidity are subsequently used to derive the absolute atmospheric temperatures and humidities.

The combined accuracy of the radiosonde telemetry system and the ground receiving and recording (strip charts) station equals the accuracy of the sensors plus 1.0% of recorder (strip chart) span. The temperature sensor's accuracy is $\pm$ .2°C from 0 to 50°C, and $\pm$ .4°C from -40 to 0°C. This accuracy combined with the 1.0% of recorder span factor results in a net $\pm$ .30°C accuracy of the final data reported. The accuracy of the humidity sensor is $\pm$ 5.5% relative humidity (R.H.), above 0°C, and in an operating range of 10 to 100% R.H. This accuracy combined with the 1.0% of recorder span factor, results in a net $\pm$ 6% R.H. accuracy of the reported data.

The response times of the sensors combined with the descent rate of the radiosonde, results in a slight error of altitude positioning. The temperature sensor has a response time of 2.5 seconds, resulting in a 62 ft. altitude error, and the humidity sensor has a response time of 1.5 seconds, resulting in a 38 ft. altitude error. In all cases of data analysis, four time constants (10 sec.) were allowed for the temperature sensor to stabilize to ambient air conditions, and two time constants (5 sec.) were allowed for the humidity sensor to stabilize. Any data prior to this, as recorded on the ground station strip charts, were not used/reported. The altitude errors of 62 and 38 ft., mentioned above, are not significant compared to a total drop range (typically 10,000 to 3,000 ft.) of the radiosonde.

The actual altitude of the radiosonde, above sea level, was derived by having a knowledge of the helicopter's altitude when the radiosonde was released, the radiosonde's descent rate (25 - 26 ft./sec.) and the rate of travel of the data strip chart recorders. In addition, the point/time of radiosonde impact with the surface could be detected by a sharp fluctuation in the data. From this point, the known descent rate, and the rate

of travel of the strip chart, were then used to reconstruct the altitude profile.

3. THERMAL BRIGHTNESS TEMPERATURE

The thermal brightness temperatures of the lake waters were measured with a Barnes PRT-5 Radiation Thermometer. This instrument senses thermal, blackbody, radiation from 8 to 14 μm; it has a sensitivity range of -20 to +75^{o}C, a field of view of 2^{o}, an accuracy of .5^{o}C, and a stability of better than 1%.

Two methods of calibration were used to calibrate the PRT-5. For temperatures below ambient temperature, a blackbody temperature equivalent was immersed in a dry ice and acetone controlled bath and allowed to stabilize for one-half hour at each temperature measured. The temperature of the bath was monitored by a stem thermometer traceable to the National Bureau of Standards. For ambient and higher temperatures, a blackbody standard, traceable to N.B.S., was allowed to stabilize at given temperatures.

The PRT-5 was simply taken aloft in helicopter in order to make rapid and thorough determinations of the lake waters. The PRT-5 sensor head was pointed directly down (nadir), out of the helicopter's door. The reference blackbody cavity control was continuously monitored in order to assure that no adverse effects on the data occurred.

4. SOLAR RADIATION - DIRECT, TOTAL, DIFFUSE, AND TARGET RADIANCE AT GROUND LEVEL

In order to derive absolute quantities of total and diffuse solar radiation, the I.S.C.O. spectroradiometer and Bendix Model 100 R.P.M.I. were calibrated with standard, tungsten strip, bulbs.* Intensity calibration factors, C.F. (I), were derived by comparing the raw outputs of the I.S.C.O. and Bendix, I_r, with that of the

*Traceable to N.B.S. and the National Research Council of Canada.

standard bulb absolute intensity, I_{std}. The desired intensity calibration factor is then

$$C.F.\ (I) = I_{std}/I_r$$

Hence, field data consisting of I_r values can be converted to absolute units by simply multiplying the raw data by the intensity calibration factor. The resultant absolute accuracy is approximately $\pm$ 5% in the 400 to 750 nm region, and $\pm$ 7% in the 750 to 1300 nm region.

For the I.S.C.O., the intensity calibration factor was derived at each wavelength increment (25 nm from 400 to 750 nm, and 50 nm from 750 to 1300 nm) of the wavelength scan. The results are shown in Figure A-1. In addition, because the I.S.C.O. was used to measure total solar radiation, the actual cosine response of the I.S.C.O. diffuser, fiber optics head, was measured. A true cosine response is defined as

$$I_\theta = I_{(\theta = o)} \cos \theta$$

where I_θ is the instrument intensity reading when the normal to the diffuser makes an angle of θ with the source (plane parallel) radiation, and $I_\theta = I_{(\theta = o)}$ is the intensity reading when the source radiation is normally incident to the diffuser. The I.S.C.O. diffuser head was positioned at angles of 0^o, 10^o, 30^o, 45^o, 60^o, and 70^o with respect to the standard bulb source, and each intensity reading at each wavelength increment of scan was recorded. A cosine response Correction Factor, C.F. (c), was derived by the following relationship

$$C.F.\ (c) = \frac{I_r(\theta = o) \cos \theta}{I_r(\theta)}$$

where $I_r(\theta = o)$ is the I.S.C.O. intensity reading when the diffuser is normal to the source, and $I_r(\theta)$ is the actual intensity reading at an angle θ. Hence, if the diffuser has a true cosine response the C.F. (c) would be equal to unity. The derived cosine response Correction Factors are shown in Figures A-2 and A-3. As can be seen, the diffuser has an excellent cosine response in the visible wavelength region; however, a very significant departure occurs at the longer wavelengths. The raw field data of total solar radiation taken with the I.S.C.O. required correction for this departure. This was done by simply multiplying the raw data by the consine response Correction Factors, for the specific solar zenith angle that occurred at the time of measurement. Hence, the I.S.C.O. raw field data for total solar radiation was converted to absolute units, I_{abs}, by the following relationship,

$$I_{abs} = I_r * C.F.\ (I) * C.F.\ (c)$$

The raw field data for diffuse solar radiation was converted to absolute units by the following relationship;

$$I_{abs} = I_r * C.F.\ (I)$$

because the diffuse sky radiation has no directional properties (hence, no cosine correction is required).

The wavelength scan of the I.S.C.O. was periodically, both in the field and laboratory, checked with a Schott BG-36 absorption filter. This filter has well defined, by a Beckman DK-2 Spectrophotometer, narrow absorption bands that were used to check the I.S.C.O. wavelength integrity. The wavelength integrity was found to be very good and accurate to approximately $\pm$ 2 nm in the 400 to 750 nm region, and $\pm$ 3 nm in the 750 to 1350 nm region.

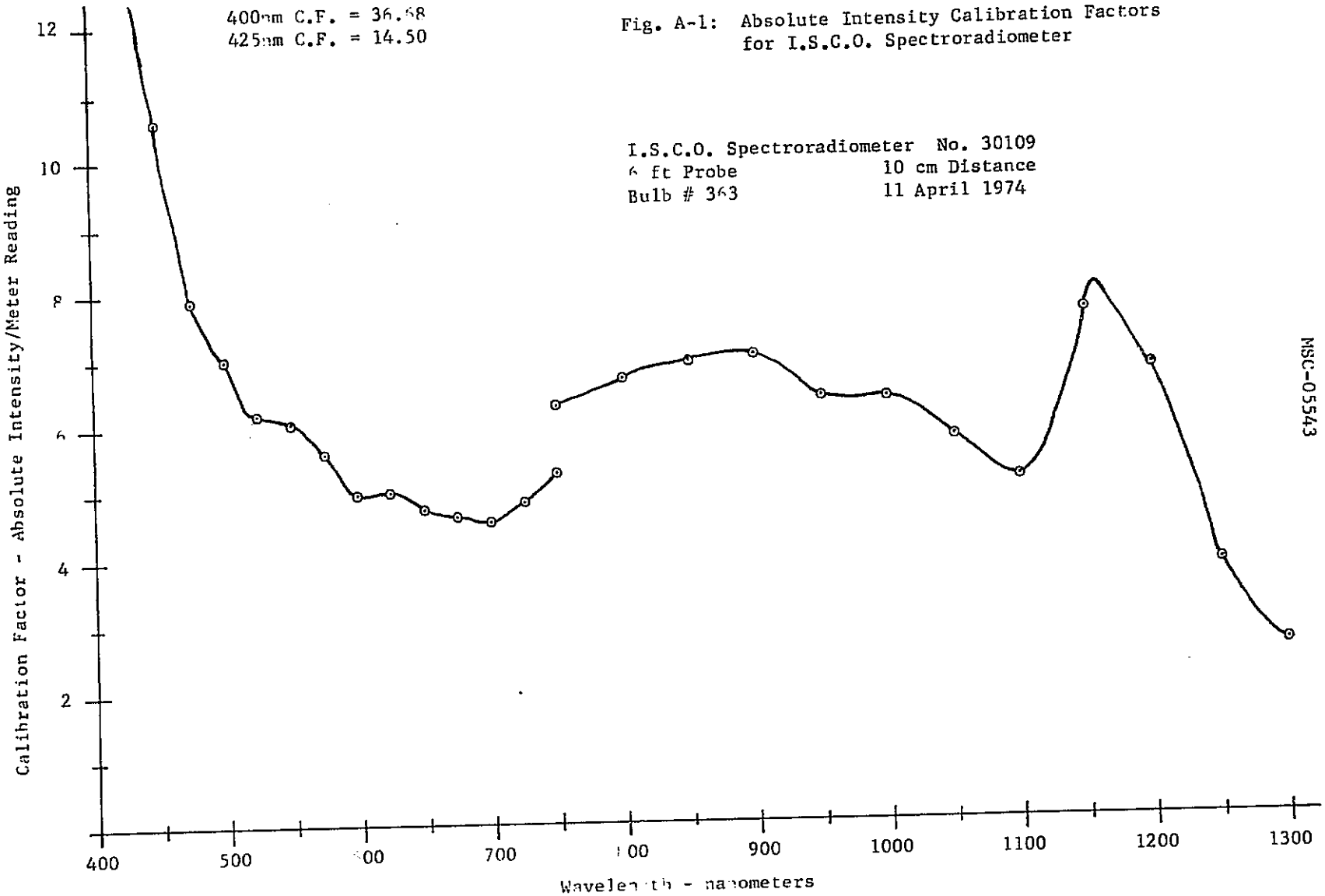

Fig. A-1: Absolute Intensity Calibration Factors for I.S.C.O. Spectroradiometer

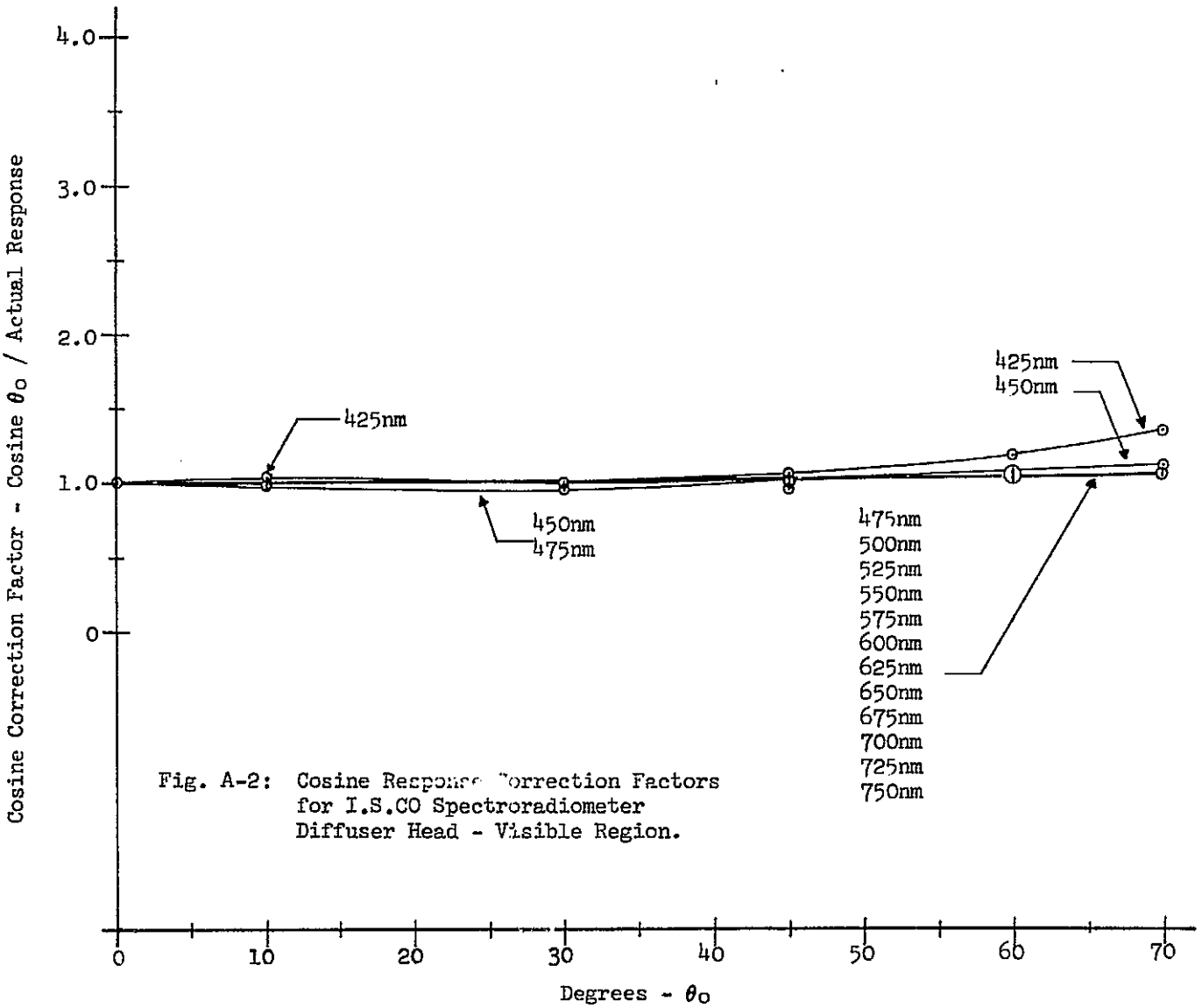

Fig. A-2: Cosine Response Correction Factors for I.S.CO Spectroradiometer Diffuser Head - Visible Region.

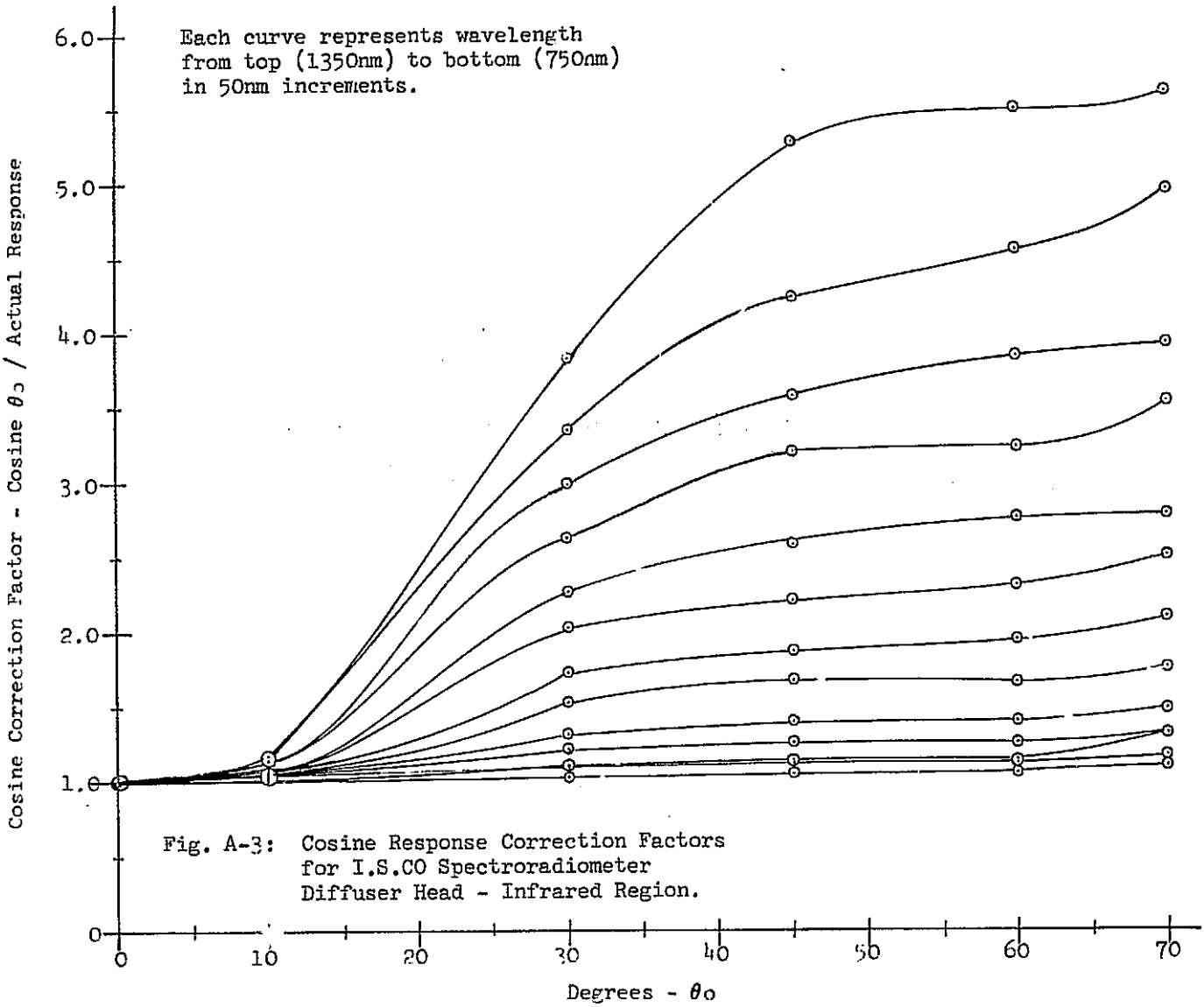

Fig. A-3: Cosine Response Correction Factors for I.S.CO Spectroradiometer Diffuser Head - Infrared Region.

As an independent check for the I.S.C.O. measurements and integrity, a field mission was performed on top of Mt. Evans, CO., 14,000 feet A.S.L. Meter readings at various air mass were obtained and used to derive a meter reading outside of the atmosphere, as described in section 3.2.3.4. This meter reading was then multiplied by the intensity calibration factors derived in the manner described above. This resulted in an absolute measurement of the solar constant. These Mt. Evans, I.S.C.O. measurements for the solar constant were then compared to those reported by M. Thekaekara, "Evaluating the Light from the Sun", Optical Spectral, March, 1972. A mean deviation (over all wavelengths) of less than 5% was obtained, as shown in Figure A-4. Both the I.S.C.O. (No. 30109) used for deriving the total and diffuse solar radiation quantities reported herein, and the I.S.C.O.(No. 17336) used for deriving optical depth, were used. The agreement between the two instruments and with the proposed standard solar constant is considered to be acceptable and within the absolute accuracy, $\pm$ 5% in the 400 to 750 nm region and $\pm$ 7% in the 750 to 1300 nm region, that is associated with the calibration techniques described previously.

The Bendix R.P.M.I. was calibrated for both total, direct, and diffuse measurements, as discussed above, and for target radiance measurements. Calibrations were performed both for the ERTS bands (B1-.500 to .600 μm, B2-.600 to .700 μm, B3-.700 to .800 μm, and B4-.800 to 1.10 μm), and for the actual/real half-bands, as shown in Figure A-5, (B1R-.505 to .590 μm, B2R-.600 to .720 μm, B3R-.680 to .815 μm, and B4R-.810 to 1.02 μm). The calibrations were adjusted for the fact, because of the broad-bands, that the calibration source spectrum (standard bulb) is different than that of the solar radiation spectrum. These bulb to solar correction(s) were performed by Bendix. The results are

Fig. A-4: Mt. Evans, CO, I.S.CO Derivations of Absolute Solar Constant.

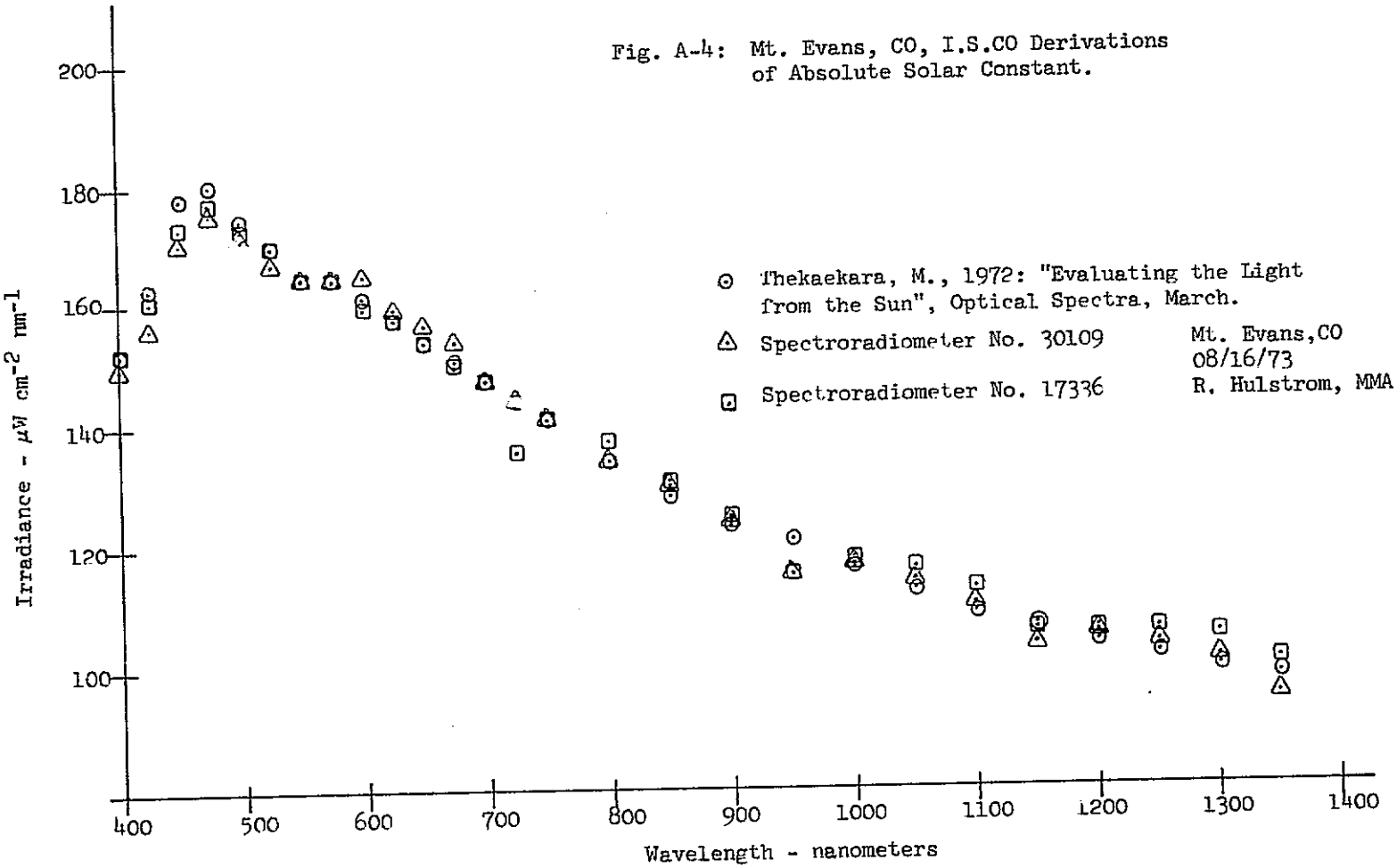

Fig. A-5: Spectral Responses of Bendix R.P.M.I. - Filters and Sensor.

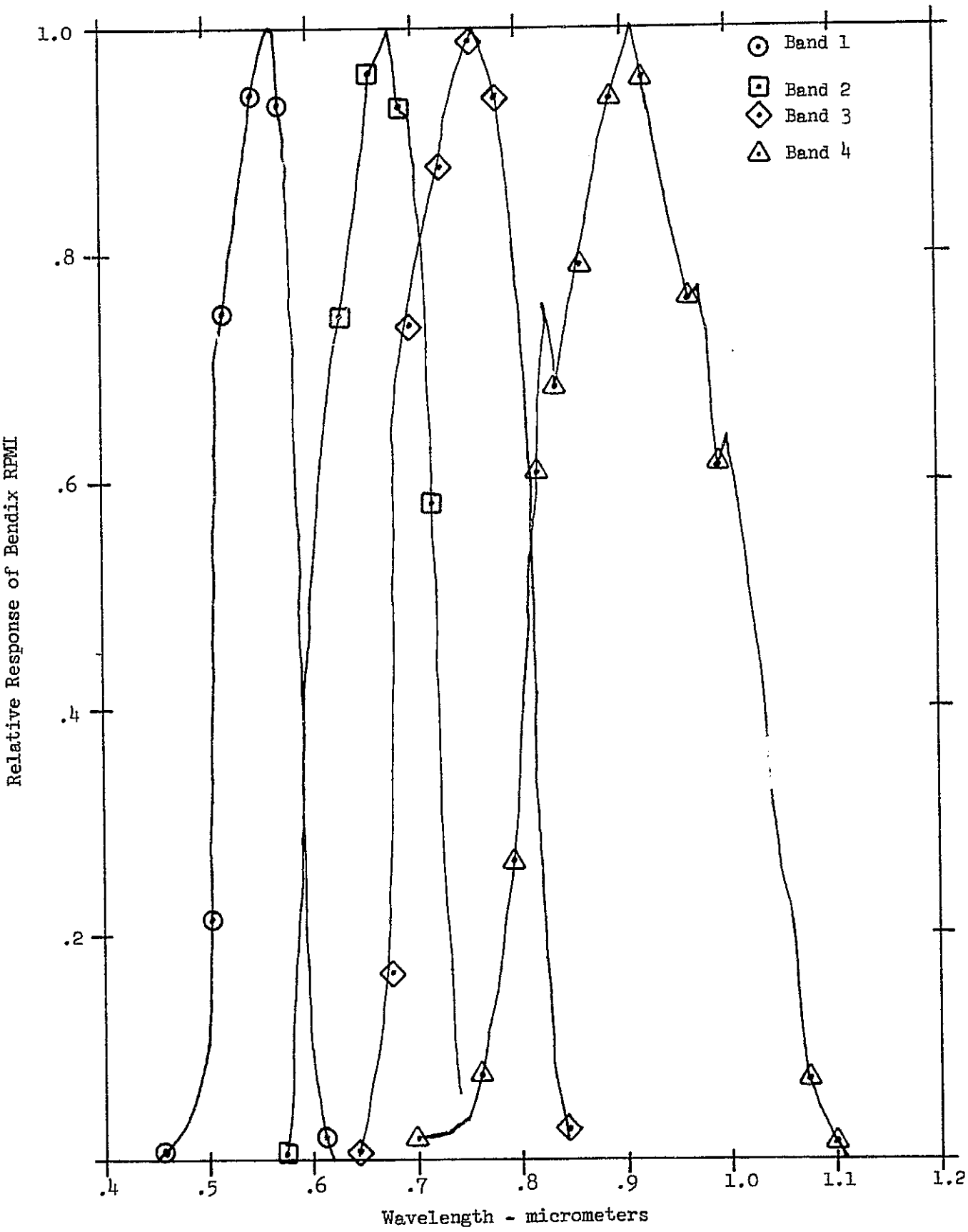

shown in Table A-1.

Table A-1

Absolute Calibration Factors of Bendix R.P.M.I.

Band	CF(I) Solar	S*	CF(I) radiance
B1	11.52	.970	895
B1R	9.59	.970	743
B2	9.80	.988	758
B2R	12.24	.988	943
B3	10.41	.985	778
B3R	14.01	.985	1079
B4	31.05	.958	2245
B4R	21.96	.958	1665

* Radiant Power Measuring Instrument for ERTS Ground Truth, Operation and Maintenance Manual for PN2373045, Bendix Aerospace Systems Division

The Bendix R.P.M.I. meter readings when multipled by $CF(I)_{solar}$ (direct, total, diffuse) result in absolute quantities of watts meter^{-2} $\Delta\lambda^{-1}$, and when multiplied by $CF(I)_{radiance}$ (viewing the target with a 7.0^{o} F.O.V. collimator) results in absolute quantities of watts meter^{-2} steradian^{-1} $\Delta\lambda^{-1}$.

The absolute accuracy of the R.P.M.I. is $\pm$ 5%. In addition, a determination of the solar constant was performed with the R.P.M.I. by Dr. R. Rogers of Bendix, resulting in a + 5.2% (R.P.M.I. value compared to solar constant) agreement for B1, a -.3% agreement for B2, a -.3% agreement for B3, and a +1.2% agreement for B4. In addition, a comparison of Calibration Factors derived by R. Hulstrom of Martin Marietta Aerospace, shown in Table A-I, with those derived by R. Rogers of Bendix Aerospace, indicates an agreement ranging

from .5% for B1 to 5% for B4. This is well within the accuracy of the calibration limitations of the methods used.

No cosine response calibration of the Bendix R.P.M.I. was performed because it was not required for analyzing the field data. The R.P.M.I. was used only on the 08 August Great Salt Lake Desert(SL-3)mission to measure total and diffuse solar radiation. The method used to derive the total solar radiation was that of measuring the direct horizontal solar radiation and adding that to the measured diffuse solar. Hence, no cosine response function was involved.

As shown in the text, it is suspected that the collimator of the R.P.M.I. introduces additional radiance to the direct measurements of target radiance. During SL-3 missions, this was detected by comparing the direct field measurements of target radiance with those obtained by deducing target radiance from measuring the incident solar radiation and the target's reflectivity. This comparison revealed that the collimator radiance attributed an additional 7-12% radiance. To verify this field measurement finding, a laboratory experiment was conducted. A plane-parallel calibration source of light was viewed with and without the collimator in place. It was found that the collimator in-place readings were 10% higher for B1, 12% higher for B2, 13% higher for B3, and 14% higher for B4. These laboratory derivations are in fair agreement with the field derivations. Therefore, the target radiance values reported throughout the main text of this report were adjusted for collimator radiance. However, it should be kept in mind that the actual magnitude of such an adjustment depends upon the incoming solar radiation conditions and target reflectivity. Due to the fact that most of the targets measured were roughly similar in reflectivities, the collimator radiance adjustments made are thought to be fairly accurate.

5. TARGET RADIANCE AT EREP

The target radiance at EREP, N_s, was determined by

$$N_s = N_t(g)\ T + N_a$$

where $N_t(g)$ is the target radiance at ground level, T is the atmospheric fractional transmittance, and N_a is the atmospheric path radiance. The target radiance at ground level can further be given by

$$N_t(g) = \frac{H\rho}{\pi}$$

where H is the total amount of solar radiation, and ρ is the target reflectivity.

The accuracy to which the target radiance at ground level is mainly determined by the accuracy to which the total solar radiation was measured. As mentioned previously, this is $\pm$ 5% in the I.S.C.O. visible and Bendix bands, and $\pm$ 7% for the I.S.C.O. infrared. The accuracy of the target reflectivity is much less of a factor because it is derived from relative instrument readings. Both the I.S.C.O. and Bendix have $\pm$ 1% meters and/or strip charts. Taking the worst case then, the accuracy of the target radiance at ground level is approximately $\pm$ 6% for the I.S.C.O. visible and Bendix bands, and $\pm$ 8% for the I.S.C.O. infrared region.

The atmospheric transmittance, T, can be given as

$$T = e^{-\tau \sec \theta}$$

where τ is the atmospheric optical depth and θ is the sensor

view angle, which was zero or near zero in all cases reported. The I.S.C.O. measurements from Mt. Evans, discussed previously, and comparisons of the Bendix and I.S.C.O. derivations of optical depth, suggest that the atmospheric optical depth measurements are consistent/accurate to within approximately $\pm$ .02 units. The optical depths reported herein ranged from approximately .600 to .100, the optical depth error of $\pm$ .02 then becomes equivalent to a $\pm$ 2% accuracy for atmospheric transmittance.

Taking the combined errors of the target radiance at ground level and the measurement of atmospheric transmittance, an accuracy of $\pm$ 8% for the 400 to 750 nm and a $\pm$ 10% for the 750 to 1300 nm region is obtained.

The accuracy/error associated with the atmospheric path radiance is difficult to assess. The use of actual field measurements of atmospheric optical depth and target reflectivity should maximize the accuracy of the computer model calculations of path radiance. A comparison of experimental path radiance measurements with model calculations is shown in Figure A-6. As can be seen, a good agreement exists. However, it is simply impossible to assign a quantitative accuracy to the path radiance derivations. Further research utilizing EREP and ERTS data is required in order to do this. Since the path radiance constitutes a major portion of the radiance derived at EREP (see Figure 24) for the shorter wavelengths, it is this region that has the highest degree of uncertainty. Since the path radiance decreases very rapidly at longer wavelengths, it is this region that has the lowest degree of uncertainty. The accuracy of the radiance derived at EREP in the infrared region (750 to 1300 nm) is approximately equal to the accuracy derived previously -- $\pm$ 10%.

Fig. A-6: Comparison of Model Calculations and Measurements of Sky Radiance - from "Studies of Spectral Discrimination", W.A. Malila, NASA CR-WRL 31650-22-T, Environmental Research Institute of Mich.

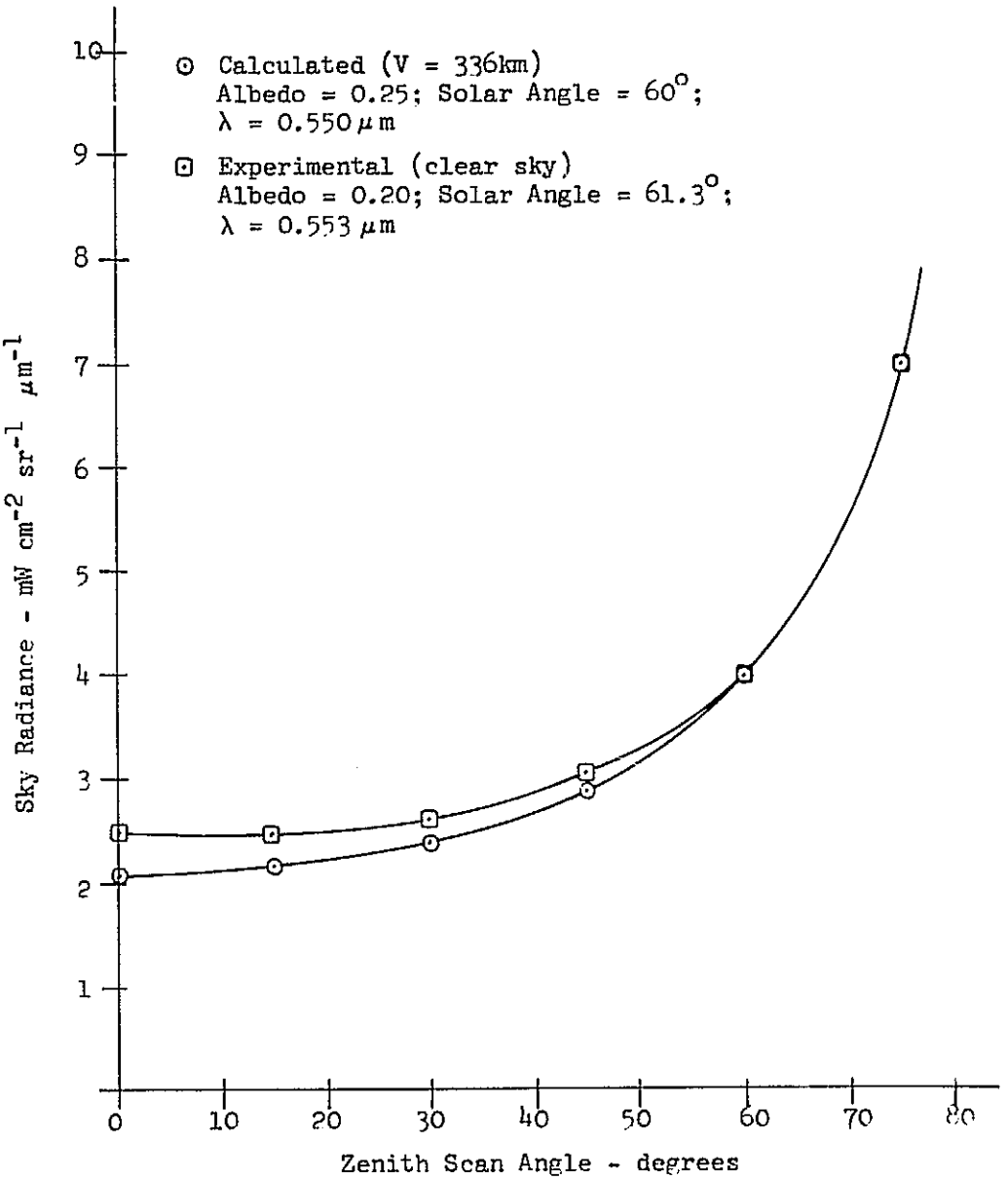

Recently the author of this report (R. Hulstrom) has had the opportunity to make direct comparisons of the path radiance determined by techniques/measurements used in this report with measurements made by the Russian "Soyuz-7" and "Soyuz-9" Spacecraft and measurements by Dr. R. Rogers. The russian spacecraft measurements were given in a letter from Dr. O. B. Vasilyev to Dr. A. F. Gregory, President of "Gregory Geoscience Ltd.", Ottawa, Canada. Copies of this letter were obtained by Dr. R. Rogers and R. Hulstrom. No details of how the Soynz measurements were made were given. The measurements by Dr. R. Rogers are explained in detail in "A Technique for Correcting ERTS Data for Solar and Atmospheric Effects", ERTS Symposium, NASA SP-322. They are basically derived by ground measurements using the model 100 R.P.M.I. to measure the sky radiance at various look-angles, and then correcting them to the ERTS situation of looking down at nadir. The comparisons are given below.

Band - B1 (.500 to .600 μm)				
Measurement	Soyuz-7	Soyuz-9	Rogers	Hulstrom*
Transmittance	.80	.84	.80	.77
Path Radiance**	2.50	1.90	3.00	2.73
Band - B2 (.600 to .700 μm)				
Measurement	Soyuz-7	Soyuz-9	Rogers	Hulstrom
Transmittance	.87	.91	.85	.84
Path Radiance	1.00	1.30	1.60	1.76
Band - B3 (.700 to .800 μm)				
Measurement	Soyuz-7	Soyuz-9	Rogers	Hulstrom
Transmittance	--	--	.89	.88
Path Radiance	--	--	1.00	1.09

* Katherine Playa (02-01-74), in this report.

** $W\ m^{-2}\ \Delta\lambda^{-1}\ sr^{-1}$

The agreement between the three independent methods is very good. However, more specifics are required to make an exact comparison.